Operating diagrams for a three-tiered microbial food web in the chemostat

Sarra Nouaoura, Radhouane Fekih-Salem, Nahla Abdellatif, Tewfik Sari

▶ **To cite this version:**

Sarra Nouaoura, Radhouane Fekih-Salem, Nahla Abdellatif, Tewfik Sari. Operating diagrams for a three-tiered microbial food web in the chemostat. Journal of Mathematical Biology, 2022, 85 (5), 10.1007/s00285-022-01812-5 . hal-03284354

HAL Id: hal-03284354
https://hal.science/hal-03284354v1

Submitted on 12 Jul 2021

HAL is a multi-disciplinary open access archive for the deposit and dissemination of scientific research documents, whether they are published or not. The documents may come from teaching and research institutions in France or abroad, or from public or private research centers.

L'archive ouverte pluridisciplinaire **HAL**, est destinée au dépôt et à la diffusion de documents scientifiques de niveau recherche, publiés ou non, émanant des établissements d'enseignement et de recherche français ou étrangers, des laboratoires publics ou privés.

OPERATING DIAGRAMS FOR A THREE-TIERED MICROBIAL FOOD WEB IN THE CHEMOSTAT

Sarra Nouaoura[a,*], Radhouane Fekih-Salem[a,c]
Nahla Abdellatif[a,d] and Tewfik Sari[b]

[a] University of Tunis El Manar, National Engineering School of Tunis, LAMSIN, 1002, Tunis, Tunisia
[b] ITAP, Univ Montpellier, INRAE, Institut Agro, Montpellier, France
[c] University of Monastir, Higher Institute of Computer Science of Mahdia, 5111, Mahdia, Tunisia
[d] University of Manouba, National School of Computer Sciences, 2010, Manouba, Tunisia

(Communicated by the associate editor name)

Abstract. In this paper, we consider a three-tiered food web model in a chemostat, including chlorophenol, phenol, and hydrogen substrates and their degraders. The model takes into account the three substrate inflowing concentrations, as well as maintenance, that is, decay terms of the species. The operating diagrams give the asymptotic behavior of the model with respect to the four operating parameters, which are the dilution rate and the three inflowing concentrations of the substrates. These diagrams were obtained only numerically in the existing literature. Using the mathematical analysis of this model obtained in our previous studies, we construct the operating diagrams, by plotting the curves that separate their various regions. Hence, the regions of the operating diagrams are constructed analytically and there is no requirement for time-consuming algorithms to generate the plots, as in the numerical method. Moreover, our method reveals behaviors that have not been detected in the previous numerical studies. The growth functions are of Monod form with the inclusion of a product inhibition term. However, our method applies for a large class of growth functions. We construct operating diagrams with and without maintenance showing the role of maintenance on the stability of the system.

1. **Introduction.** The anaerobic digestion (AD) process is of increasing interest since it is able to produce renewable energy while treating waste/wastewater. Understanding and exploiting this process appears to be a major challenge to tackle contemporary issues in the field of wastewater treatments and the development of renewable energy, and to improve next future bioprocesses.

The generic AD model No.1 (ADM1) developed in [3] is characterized by its extreme complexity with 32 state variables and a large number of parameters. A

2010 *Mathematics Subject Classification.* Primary: 34A34, 34D20; Secondary: 92B05, 92D25.
Key words and phrases. Anaerobic digestion, operating diagram, chemostat, limit cycle, Hopf bifurcation, three-tiered food web.
This work was supported by the Euro-Mediterranean research network TREASURE (http://www.inra.fr/treasure).
* Corresponding author: Sarra Nouaoura.

simple two-step AD model (called AM2) proposed by [6] provides satisfactory prediction of the AD process and demonstrates the ability to reproduce the experimental data and the dynamical behavior. Many papers in the literature have studied the AM2 model (see [4, 7, 11, 14, 17, 24, 25, 27, 33] and the reference therein).

A mathematical model of a chlorophenol-mineralizing three-tiered microbial "food web" has been proposed by Wade et al. [30], by introducing an additional microorganism and substrate into a two-tiered feeding chain model considered by Xu et al. [33]. Since the chlorophenol mineralization may occur under aerobic or anaerobic conditions with different microbial consortia involved, the three-tiered food-web is a generic model that is also found in anaerobic digestion. The organisms involved in the resulting three-tiered model are the chlorophenol-dechlorinating bacterium, the phenol degrader and the hydrogenotrophic methanogen. Several authors studied the three-tiered model, see [12, 21, 20, 26, 29, 30]. Using specific growth rates, Wade et al. [30] have proven that the model can have up to eight steady states. Sari and Wade [26], have considered the case with only chlorophenol input substrate and general growth rates. The existence of the steady states has been characterized analytically. It was shown that the stability conditions can be explicitly determined, in the case without maintenance terms. In [29], the original three-tiered model of [26, 30] was considered in the case neglecting maintenance. The authors confirmed the existence of eight steady states and proved analytically the persistence of the model when maintenance is excluded. In [21], we have extended the results of [26] by considering the phenol and hydrogen inflowing concentrations. We have analytically determined the necessary and sufficient conditions of the existence of the steady states in the case with maintenance. The necessary and sufficient conditions of the local stability are performed analytically when maintenance is excluded. Then, these results of local stability are extended in [20] to the case where maintenance is included. Using a large class of growth functions, we have provided rigorous proofs for the results of [30] on the existence and stability of the steady states, which, for the most part, were obtained only numerically and for specific kinetics in [30].

In this work, we consider the three-tiered model proposed in [30], and we are interested to complete the mathematical analysis of this model by studying theoretically the operating diagrams. Using the existence and stability conditions of all steady states determined analytically in [20, 21], our main contribution in this paper is the construction of the operating diagrams, by plotting the curves which separate their different regions, in both cases with and without considering decay terms. The operating diagram shows the dynamic behavior of the system according to the conventional chemostat operating parameters (the dilution rate and the input concentrations of the substrates) such that the values of the biological parameters are fixed. It is the best tool for biologists since it allows to predict qualitatively the different asymptotic behaviors of the process according to its control parameters. As it was claimed in [28], the operating diagram remains the most useful answer for the analysis of the behavior of the model according to the parameters. This diagram is often performed both in the biological literature [22, 27, 30, 33] and the mathematical literature [1, 2, 7, 8, 9, 10, 13, 14, 15, 16, 17, 19, 23, 25, 26, 32, 31].

In [30], the operating diagrams have been constructed numerically with a resolution of 5000×5000 solution points. The authors determined numerically the steady states for a realistic range of operational and kinetic parameters. Using Matlab, they solve complex polynomials to calculate the components of the steady states

and the characteristic polynomials to determine which are stable. By considering sets of operating parameters and repeating this method with numerous ones, the diagrams are drawn, showing the region of stability of each steady state. Nevertheless, the operating diagrams plotted in [30], with respect to the concentration of chlorophenol and the dilution rate did not depict all the behavior of the model. More precisely, the destabilization of the positive steady state via a Hopf bifurcation with the emergence of a stable limit cycle had not been observed. In [26], the operating diagrams were obtained, analytically in the case without maintenance and numerically in the case with maintenance. The authors were able to provide analytical expressions of the boundaries between the different stability regions allowing to give operating diagrams describing the exhaustive behavior of the system. Adding the maintenance terms, they highlighted by a numerical stability analysis the presence of the region of instability of the positive steady state and showed the possibility of a Hopf bifurcation, with the appearance of a stable limit cycle which were not depicted in [30], a fact that were confirmed in [29] in the case where the maintenance terms are neglected.

The one parameter bifurcation diagrams of the three-tiered model presented in [20, 21] were analytically constructed in the cases with and without maintenance. They show that the model has in both cases rich dynamics including bistability, coexistence and occurrence of the limit cycle due to supercritical Hopf bifurcation.

In this paper, we describe analytically the operating diagrams and we highlight the impact of the maintenance terms and the importance of the phenol and hydrogen input concentrations, on the asymptotic behavior of the model. We compare our results with the findings of previous numerical analysis in [30] where several regions have been omitted.

The paper is organized as follows. In section 2, we present the mathematical model of three-tiered microbial species of [30]. Next, in section 3, we describe analytically the operating diagrams in both cases with and without maintenance terms. First, with respect to the chlorophenol input substrate concentration and the dilution rate and second, with respect to the hydrogen and the phenol input substrate concentrations. Finally, we discuss our results and we give some conclusions in section 4. In Appendix A, we present the change of variables that are used to simplify the analysis of the general model and we describe the results of [20, 21] on the existence and local stability of the steady states. Numerical computations are reported in Appendices B and C. The equations of the surfaces that delimit the regions of the operating diagrams are provided in Appendix D.

2. **Mathematical model.** The three-tiered microbial food web model, considered in [30], can be written as follows:

$$\begin{cases} \dot{X}_{\mathrm{ch}} &= (Y_{\mathrm{ch}} f_0\left(S_{\mathrm{ch}}, S_{\mathrm{H_2}}\right) - D - k_{\mathrm{dec,ch}}) X_{\mathrm{ch}} \\ \dot{X}_{\mathrm{ph}} &= (Y_{\mathrm{ph}} f_1\left(S_{\mathrm{ph}}, S_{\mathrm{H_2}}\right) - D - k_{\mathrm{dec,ph}}) X_{\mathrm{ph}} \\ \dot{X}_{\mathrm{H_2}} &= (Y_{\mathrm{H_2}} f_2\left(S_{\mathrm{H_2}}\right) - D - k_{\mathrm{dec,H_2}}) X_{\mathrm{H_2}} \\ \dot{S}_{\mathrm{ch}} &= D\left(S_{\mathrm{ch}}^{\mathrm{in}} - S_{\mathrm{ch}}\right) - f_0\left(S_{\mathrm{ch}}, S_{\mathrm{H_2}}\right) X_{\mathrm{ch}} \\ \dot{S}_{\mathrm{ph}} &= D\left(S_{\mathrm{ph}}^{\mathrm{in}} - S_{\mathrm{ph}}\right) + \frac{224}{208}\left(1 - Y_{\mathrm{ch}}\right) f_0\left(S_{\mathrm{ch}}, S_{\mathrm{H_2}}\right) X_{\mathrm{ch}} - f_1\left(S_{\mathrm{ph}}, S_{\mathrm{H_2}}\right) X_{\mathrm{ph}} \\ \dot{S}_{\mathrm{H_2}} &= D\left(S_{\mathrm{H_2}}^{\mathrm{in}} - S_{\mathrm{H_2}}\right) - \frac{16}{208} f_0\left(S_{\mathrm{ch}}, S_{\mathrm{H_2}}\right) X_{\mathrm{ch}} + \frac{32}{224}(1 - Y_{\mathrm{ph}}) f_1\left(S_{\mathrm{ph}}, S_{\mathrm{H_2}}\right) X_{\mathrm{ph}} \\ & \quad - f_2(S_{\mathrm{H_2}}) X_{\mathrm{H_2}}, \end{cases} \tag{1}$$

where S_{ch}, S_{ph} and $S_{\mathrm{H_2}}$ are the chlorophenol, phenol and hydrogen substrate concentrations, respectively. X_{ch}, X_{ph} and $X_{\mathrm{H_2}}$ denote, the chlorophenol, phenol and

hydrogen degrader concentrations. D is the dilution rate. f_i, $i = 0, 1, 2$ are the specific growth rates, $S_{\text{ch}}^{\text{in}}, S_{\text{ph}}^{\text{in}}$ and $S_{\text{H}_2}^{\text{in}}$ are the inflowing concentrations in the chemostat, $k_{\text{dec,ch}}, k_{\text{dec,ph}}$ and $k_{\text{dec,H}_2}$ represent the maintenance (or decay) rates, and Y_{ch}, Y_{ph} and Y_{H_2} are the yield coefficients. The value $224/208\,(1 - Y_{\text{ch}})$ represents the fraction of chlorophenol converted to phenol, $32/224\,(1 - Y_{\text{ph}})$ is the fraction of phenol that is transformed to hydrogen and $16/208$ represents the fraction of hydrogen consumed by the chlorophenol degrader X_{ch}.

The growth functions take the following form:

$$\begin{aligned} f_0\,(S_{\text{ch}}, S_{\text{H}_2}) &= \frac{k_{m,\text{ch}} S_{\text{ch}}}{K_{S,ch} + S_{\text{ch}}} \frac{S_{H_2}}{K_{S,\text{H}_2,c} + S_{\text{H}_2}}, \\ f_1\,(S_{\text{ph}}, S_{\text{H}_2}) &= \frac{k_{m,\text{ph}} S_{\text{ph}}}{K_{S,\text{ph}} + S_{\text{ph}}} \frac{1}{1 + S_{\text{H}_2}/K_{I,\text{H}_2}}, \quad f_2\,(S_{\text{H}_2}) = \frac{k_{m,\text{H}_2} S_{\text{H}_2}}{K_{S,\text{H}_2} + S_{\text{H}_2}}. \end{aligned} \tag{2}$$

The mathematical analysis of (1) given in [20, 21, 26] is carried out with a general class of growth functions, of which functions (2) are a particular example. Under these assumptions, system (1) can have up to eight steady states labelled as in [30] by $\text{SS1}, \text{SS2}, \ldots, \text{SS8}$ and detailed as follows:

- SS1: the washout steady state where all populations are extinct.
- SS2: only the hydrogenotrophic methanogens are maintained ($X_{\text{H}_2} > 0$).
- SS3: only the chlorophenol degraders are maintained ($X_{\text{ch}} > 0$).
- SS4: only the hydrogenotrophic methanogens are washed out (X_{ch} and $X_{\text{ph}} > 0$).
- SS5: only the phenol degraders are washed out (X_{ch} and $X_{\text{H}_2} > 0$).
- SS6: all three populations are present (X_{ch}, X_{ph} and $X_{\text{H}_2} > 0$).
- SS7: only the phenol degraders are present ($X_{\text{ph}} > 0$).
- SS8: only the chlorophenol degraders are washed out (X_{ph} and $X_{\text{H}_2} > 0$).

The components of these steady states are given in Table 6, the conditions of their existence and stability are provided in Table 7.

Remark 1. The steady state SS1 always exists. There exist at most two steady states of the form SS4, that we denote by SS4^1 and SS4^2. The other steady states are unique if they exist (see Appendix A and [20, 21]).

3. Operating diagrams.

The operating diagrams show how behaves the system when the operating parameters D, $S_{\text{ch}}^{\text{in}}$, $S_{\text{ph}}^{\text{in}}$ and $S_{\text{H}_2}^{\text{in}}$ are varying in (1). To plot the operating diagrams, we must fix the values of the biological parameters and two of the four operating parameters D, $S_{\text{ch}}^{\text{in}}$, $S_{\text{ph}}^{\text{in}}$ and $S_{\text{H}_2}^{\text{in}}$. The biological parameter values used for plotting the operating diagrams are provided in Table 10 of [21]. These parameter values were used also in [20, 26, 30]. In what follows, we study the operating diagrams of system (1) in the cases with and without maintenance terms. In section 3.1, we fix $S_{\text{ph}}^{\text{in}}$ and $S_{\text{H}_2}^{\text{in}}$ and we determine the operating diagrams in the plane $\left(S_{\text{ch}}^{\text{in}}, D\right)$, and in section 3.2, we give the operating diagrams in the $\left(S_{\text{H}_2}^{\text{in}}, S_{\text{ph}}^{\text{in}}\right)$-plane, where $S_{\text{ch}}^{\text{in}}$ and D being constant.

First, from Table 7, we define in Table 9 the surfaces Γ_i, $i = 1, \ldots, 18$ which delimite the different regions of the $\left(S_{\text{ch}}^{\text{in}}, S_{\text{ph}}^{\text{in}}, S_{\text{H}_2}^{\text{in}}, D\right)$-space.

3.1. Operating diagrams in the $\left(S_{\text{ch}}^{\text{in}}, D\right)$ plane when $S_{\text{ph}}^{\text{in}}$ and $S_{\text{H}_2}^{\text{in}}$ are fixed.

Giving fixed values for $S_{\text{ph}}^{\text{in}}$ and $S_{\text{H}_2}^{\text{in}}$, the intersections of the surfaces Γ_i, $i = 1, \ldots, 14$ with the $\left(S_{\text{ch}}^{\text{in}}, D\right)$-plane are curves of functions of D. However, the intersections of surfaces Γ_i, $i = 15, \ldots, 18$ with the $\left(S_{\text{ch}}^{\text{in}}, D\right)$-plane are straight lines. Following [30],

we consider several cases to examine the effect of the operating parameters $S_{\text{ph}}^{\text{in}}$ and $S_{\text{H}_2}^{\text{in}}$ on the behavior of the model, in the cases with and without maintenance. First, only chlorophenol input is added to the system ($S_{\text{ph}}^{\text{in}} = S_{\text{H}_2}^{\text{in}} = 0$). Then, the hydrogen input is added to the system and the phenol input is excluded, ($S_{\text{ph}}^{\text{in}} = 0$ and $S_{\text{H}_2}^{\text{in}} > 0$). Next, the phenol input is added and the hydrogen input is excluded, ($S_{\text{ph}}^{\text{in}} > 0$ and $S_{\text{H}_2}^{\text{in}} = 0$). Finally, the hydrogen and phenol inputs are added to the system, ($S_{\text{ph}}^{\text{in}} > 0$ and $S_{\text{H}_2}^{\text{in}} > 0$).

3.1.1. *Only chlorophenol is in the input.* Assume that $S_{\text{ch}}^{\text{in}} > 0$, $S_{\text{ph}}^{\text{in}} = S_{\text{H}_2}^{\text{in}} = 0$. In this case, system (1) has only the steady states SS1, SS4^1, SS4^2 and SS6, see Table 7. The operating diagram in the plane $\left(S_{\text{ch}}^{\text{in}}, D\right)$ is shown in Fig. 1. Fig. 1(a) looks very similar to Fig. 1(b) except near of the origin, as it is shown in the magnifications at the right of Fig. 1(a)–(b). In the case with maintenance, the value of $S_{\text{ch}}^{\text{in}}$, in which the positive steady state SS6 is destabilized is greater than in the case without maintenance. These results are supported by numerical experimentation and are proven in Appendix B. Note that, each region that has a different asymptotic behavior is colored by a distinct color as in [30].

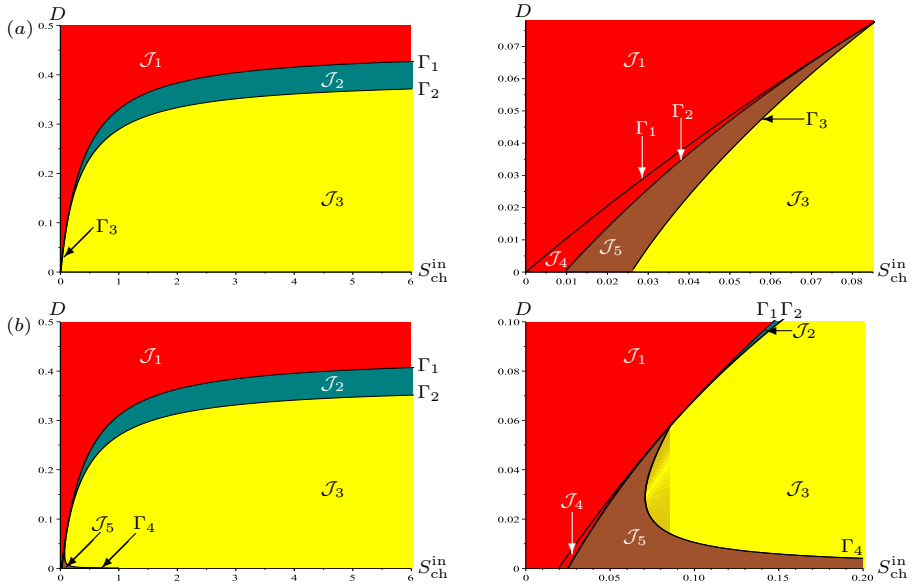

FIGURE 1. Operating diagrams in the plane $\left(S_{\text{ch}}^{\text{in}}, D\right)$, when $S_{\text{ph}}^{\text{in}} = S_{\text{H}_2}^{\text{in}} = 0$: (a) case without maintenance and on the right its magnification showing the regions $\mathcal{J}_4$ and $\mathcal{J}_5$, (b) case with maintenance and on the right its magnification showing the regions $\mathcal{J}_4$ and $\mathcal{J}_5$.

The existence and the stability of the steady states of (1) in the five regions $\mathcal{J}_i$, $i = 1, \ldots, 5$, of the operating diagrams of Fig. 1 are determined in Table 1.

Remark 2. Each region is denoted by its steady states, indicating which are stable and which are unstable. For instance, the region $\mathcal{J}_2 = (14^2, 4^1)$ in Table 1 means that when the operating parameters are taken in $\mathcal{J}_2$, then the steady states SS1 and SS4^2 are stable, the steady state SS4^1 is unstable, and there is no other steady state (SS6 does not exist).

TABLE 1. Existence and stability of steady states in the regions of the operating diagrams of Fig. 1 when $S_{\text{ph}}^{\text{in}} = S_{\text{H}_2}^{\text{in}} = 0$. The letter S (resp. U) means that the corresponding steady state is LES (resp. unstable). No letter means that the steady state does not exist.

Region	SS1	SS4^1	SS4^2	SS6	Color
$\mathcal{J}_1 = (1)$	S				Red
$\mathcal{J}_2 = (14^2, 4^1)$	S	U	S		Teal
$\mathcal{J}_3 = (16, 4^1 4^2)$	S	U	U	S	Yellow
$\mathcal{J}_4 = (1, 4^1 4^2)$	S	U	U		Red
$\mathcal{J}_5 = (1, 4^1 4^2 6)$	S	U	U	U	Sienna

When $S_{\text{ch}}^{\text{in}} > 0$ and $S_{\text{ph}}^{\text{in}} = S_{\text{H}_2}^{\text{in}} = 0$, from Table 1 and Fig. 1, we can deduce that there are no new regions that emerge under the influence of the maintenance terms. Moreover, Fig. 1(b) corresponds to Fig. 2 in [30] and highlights the existence of the region $\mathcal{J}_5$ of instability of SS6, a fact that was not reported in [30]. Actually, the behavior of the system when $S_{\text{ph}}^{\text{in}} = S_{\text{H}_2}^{\text{in}} = 0$ was already clarified in [26], where the instability of SS6 has been studied analytically in the case without maintenance, but only numerically in the case including maintenance. In fact, Fig. 1(a) is the same as Fig. 4 in [26]. Both figures are obtained analytically by plotting the curves separating the regions $\mathcal{J}_k$ from the existence and stability conditions which depend on the operating parameters. However, although Fig. 1(b) shows the same behavior as Fig. 9 in [26] achieved only numerically, our operating diagram is obtained analytically (see Appendix B). Thus, our theoretical study confirms the numerical findings presented in [26], in the case including maintenance.

3.1.2. *Hydrogen is added in the input.* Assuming that the inflowing concentrations $S_{\text{ph}}^{\text{in}} = 0$ and $S_{\text{H}_2}^{\text{in}} = 2.67 \times 10^{-5}$ are those of Fig. 3(a) in [30], we determine the operating diagrams in the $\left(S_{\text{ch}}^{\text{in}}, D\right)$-plane in both cases with and without maintenance. In this case, system (1) has further three steady states SS2, SS3 and SS5, see Table 7. Fig. 2(a) represents the operating diagram in the plane $\left(S_{\text{ch}}^{\text{in}}, D\right)$, in the case without maintenance. The three magnifications shown in Fig. 2(b)–(d) put in evidence the regions $\mathcal{J}_8$, $\mathcal{J}_{10}$ and $\mathcal{J}_i$, $i = 12, \ldots, 21$. Fig. 2 is obtained analytically by plotting the curves separating the regions and is supported by numerical experimentation (see Appendix C). Fig. 3(a) represents the operating diagram in the $\left(S_{\text{ch}}^{\text{in}}, D\right)$-plane, in the case with maintenance. The magnifications presented in Fig. 3(b)–(d) show that the regions $\mathcal{J}_1$ and $\mathcal{J}_i$, $i = 6, \ldots, 13$ are similar to those in Fig. 2. In fact, the operating diagram of Fig. 3 is determined analytically as Fig. 2 using the same method shown in Appendix C. For the sake of brevity, we do not give the numerical experimentations and the details for Fig. 3 as well as for all remaining operating diagrams in Figs. 4 to 9 since they can be obtained similarly. The addition of hydrogen input substrate leads to the occurrence of sixteen new regions besides the region $\mathcal{J}_1$ which is identical to that of the operating diagrams in Fig. 1. The existence and the stability of the steady states of (1) in the seventeen regions $\mathcal{J}_1$ and $\mathcal{J}_i$, $i = 6, \ldots, 21$, of the operating diagrams in Figs. 2 and 3, are determined in Table 2.

Our theoretical study of the operating diagrams shows the emergence of new regions which are not reported in Fig. 3(a) of [30], namely the region $\mathcal{J}_8$ of the stability of SS5 and the region $\mathcal{J}_{13}$ of the stability of SS3 with the instability of SS6. Since these regions $\mathcal{J}_8$ and $\mathcal{J}_{13}$ are very thin for the set of parameters, they

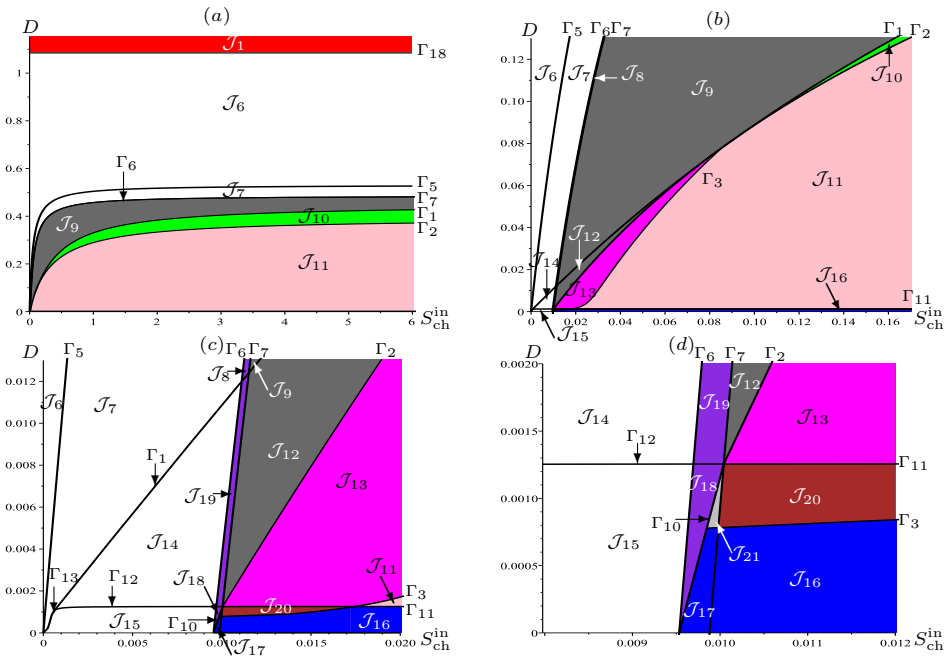

FIGURE 2. Operating diagram in the plane $\left(S^{\text{in}}_{\text{ch}}, D\right)$, when $S^{\text{in}}_{\text{ph}} = 0$, $S^{\text{in}}_{\text{H}_2} = 2.67\times10^{-5}$ and $k_{\text{dec,i}} = 0$. Magnifications (b) for $D \in [0, 0.13]$ showing the regions $\mathcal{J}_i$, $i = 12, \ldots, 16$, (c) for $D \in [0, 0.013]$ showing the regions $\mathcal{J}_8$ and $\mathcal{J}_i$, $i = 17, \ldots, 20$, (d) for $D \in [0, 0.002]$ showing the region $\mathcal{J}_{21}$.

TABLE 2. Existence and stability of steady states in the regions of the operating diagrams of Figs. 2 and 3.

Region	SS1	SS2	SS3	SS4[1]	SS4[2]	SS5	SS6	Color
$\mathcal{J}_1 = (1)$	S							Red
$\mathcal{J}_6 = (2, 1)$	U	S						White
$\mathcal{J}_7 = (2, 13)$	U	S	U					White
$\mathcal{J}_8 = (5, 123)$	U	U	U			S		Blueviolet
$\mathcal{J}_9 = (3, 12)$	U	U	S					Dimgray
$\mathcal{J}_{10} = (34^2, 124^1)$	U	U	S	U	S			Green
$\mathcal{J}_{11} = (36, 124^1 4^2)$	U	U	S	U	U		S	Pink
$\mathcal{J}_{12} = (3, 124^1 4^2)$	U	U	S	U	U			Dimgray
$\mathcal{J}_{13} = (3, 124^1 4^2 6)$	U	U	S	U	U		U	Magenta
$\mathcal{J}_{14} = (2, 134^1 4^2)$	U	S	U	U	U			White
$\mathcal{J}_{15} = (2, 134^2)$	U	S	U		U			White
$\mathcal{J}_{16} = (6, 1234^2)$	U	U	U		U		S	Blue
$\mathcal{J}_{17} = (6, 1234^2 5)$	U	U	U		U	U	S	Blue
$\mathcal{J}_{18} = (5, 1234^2)$	U	U	U		U	S		Blueviolet
$\mathcal{J}_{19} = (5, 1234^1 4^2)$	U	U	U	U	U	S		Blueviolet
$\mathcal{J}_{20} = (., 1234^2 6)$	U	U	U		U		U	Brown
$\mathcal{J}_{21} = (., 1234^2 56)$	U	U	U		U	U	U	Silver

were not detected in the numerical analysis of the operating diagram of Fig. 3(a) in [30]. In the region $\mathcal{J}_{13}$, close to the boundary with $\mathcal{J}_{11}$, the system exhibits a bistability behavior between SS3 and a stable limit cycle that emerges through a

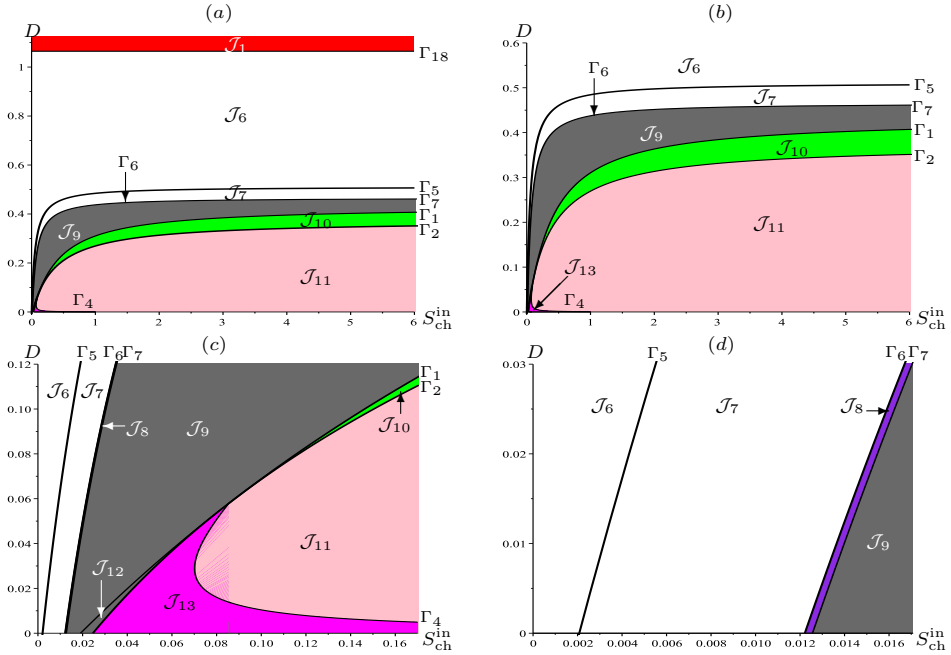

FIGURE 3. Operating diagram in the plane $\left(S^{in}_{ch}, D\right)$, when $S^{in}_{ph} = 0$ and $S^{in}_{H_2} = 2.67 \times 10^{-5}$ with maintenance. Magnifications (b) for $D \in [0, 0.6]$, (c) for $D \in [0, 0.12]$ showing the regions $\mathcal{J}_{12}$ and $\mathcal{J}_{13}$, (d) for $D \in [0, 0.03]$ showing the region $\mathcal{J}_8$.

Hopf bifurcation at the positive steady state by crossing the surfaces Γ_3 and Γ_4 from $\mathcal{J}_{11}$ to $\mathcal{J}_{13}$ in the case without and with mortality, respectively, (see Figs. 2 and 3). Note that all the steady states are unstable in the regions $\mathcal{J}_{20}$ and $\mathcal{J}_{21}$, where the numerical simulations can show that the solutions converge to a periodic orbit for any positive initial conditions. In the case with maintenance, the regions $\mathcal{J}_i$, $i = 14, \ldots, 21$ are empty. Thus, the maintenance has an effect on the disappearance of some regions.

For very low values of D, in the case without maintenance, there cannot be any destabilization of SS6 via a Hopf bifurcation because of the existence of regions $\mathcal{J}_{15}$ to $\mathcal{J}_{19}$ (where SS6 does not exist or is stable) below regions $\mathcal{J}_{13}$, $\mathcal{J}_{20}$ and $\mathcal{J}_{21}$ (where SS6 is unstable). However, in the case with maintenance, there can always be occurrence of a limit cycle for low values of D because the curve Γ_4 has the S^{in}_{ch} axis as a horizontal asymptote and separates the two regions $\mathcal{J}_{11}$ and $\mathcal{J}_{13}$ (see Fig. 3).

3.1.3. *Phenol is added in the input.* Considering the input concentrations $S^{in}_{ph} = 10^{-2}$ and $S^{in}_{H_2} = 0$ as those of Fig. 5(a) in [30], we construct the operating diagrams in the $\left(S^{in}_{ch}, D\right)$-plane in both cases with and without maintenance terms. In this case, system (1) has further two steady states SS7 and SS8. However, the steady states SS2, SS3 and SS5 do not exist since $S^{in}_{H_2} = 0$, see Table 7. Figs. 4(a) and 5(a) represent the operating diagrams in the plane $\left(S^{in}_{ch}, D\right)$, in the cases without and with maintenance, respectively. The magnifications shown in Fig. 4(b)–(c) put in evidence the regions $\mathcal{J}_i$, $i = 22, \ldots, 30$. The magnification presented in Fig. 5(b)

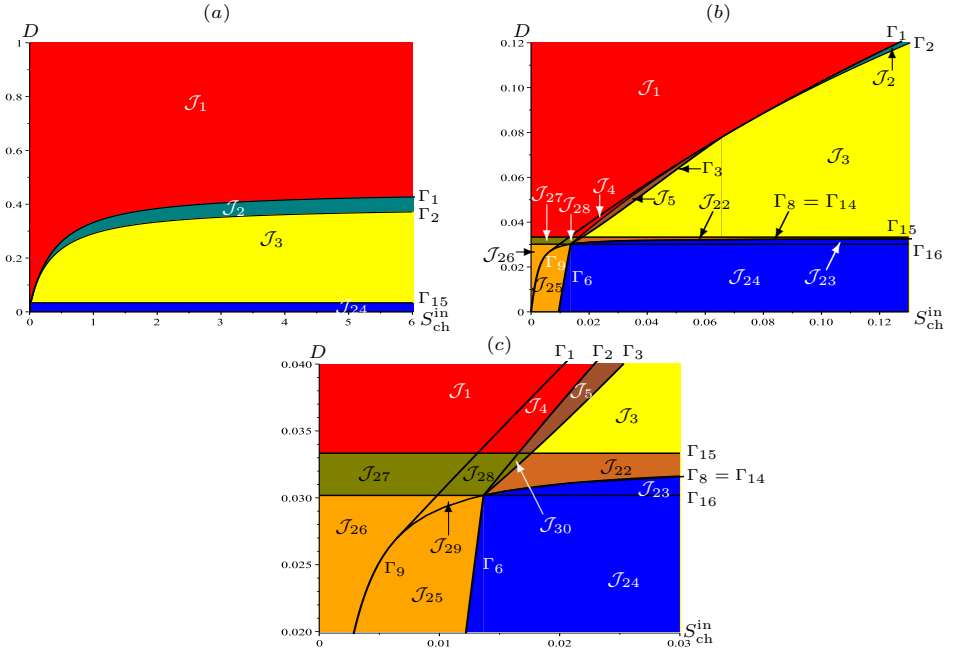

FIGURE 4. Operating diagram in the plane $\left(S^{in}_{ch}, D\right)$, when $S^{in}_{ph} = 10^{-2}$, $S^{in}_{H_2} = 0$ and $k_{dec,i} = 0$. Magnifications (b) for $D \in [0, 0.12]$ showing the regions $\mathcal{J}_i$,for $i = 22, \ldots, 28$, (c) for $D \in [0.02, 0.04]$ showing the regions $\mathcal{J}_{29}$ and $\mathcal{J}_{30}$.

shows that the regions $\mathcal{J}_i$, $i = 1, \ldots, 5, 22, \ldots, 30$ are similar to those in Fig. 4. The addition of phenol input substrate leads to the emergence of twelve new regions $\mathcal{J}_i$, $i = 22, \ldots, 32$, besides the regions $\mathcal{J}_i$, $i = 1, \ldots, 5$ which are identical to those of the operating diagrams in Fig. 1. The existence and the stability of the steady states of (1) in the sixteen regions $\mathcal{J}_i$, $i = 1, \ldots, 5, 22, \ldots, 32$ of the operating diagrams of Figs. 4 and 5 are summarized in Table 3.

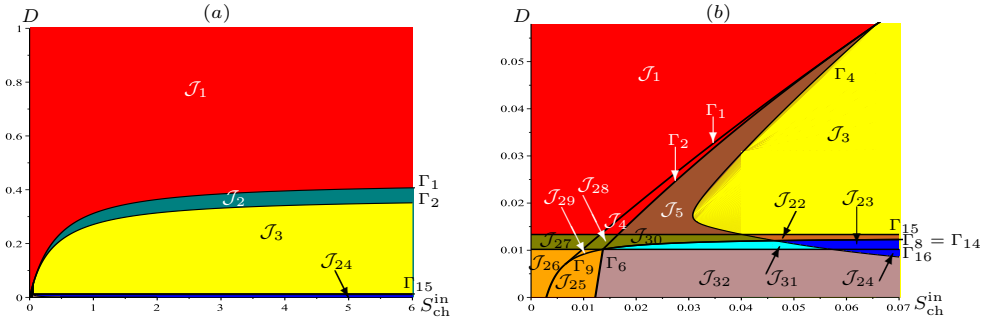

FIGURE 5. Operating diagram in the plane $\left(S^{in}_{ch}, D\right)$, when $S^{in}_{ph} = 10^{-2}$, $S^{in}_{H_2} = 0$ and $k_{dec,i} > 0$. Magnification (b) for $D \in [0, 0.058]$ showing the regions $\mathcal{J}_i$, for $i = 4, 5, 22, \ldots, 32$.

Our theoretical study of the operating diagrams in the case with phenol addition in the input shows the occurrence of new asymptotic behaviors which are not detected in Fig. 5(a) of [30]: namely, the region $\mathcal{J}_{22}$ of the bistability between SS6 and SS7, which appears in a small area between $\mathcal{J}_3$ and $\mathcal{J}_{23}$, and the regions

TABLE 3. Existence and stability of steady states in the regions of the operating diagrams of Figs. 4 and 5.

Region	SS1	SS4^1	SS4^2	SS6	SS7	SS8	Color
$\mathcal{J}_1 = (1)$	S						Red
$\mathcal{J}_2 = (14^2, 4^1)$	S	U	S				Teal
$\mathcal{J}_3 = (16, 4^1 4^2)$	S	U	U	S			Yellow
$\mathcal{J}_4 = (1, 4^1 4^2)$	S	U	U				Red
$\mathcal{J}_5 = (1, 4^1 4^2 6)$	S	U	U	U			Sienna
$\mathcal{J}_{22} = (67, 14^1 4^2)$	U	U	U	S	S		Chocolate
$\mathcal{J}_{23} = (6, 14^2 7)$	U		U	S	U		Blue
$\mathcal{J}_{24} = (6, 14^2 78)$	U		U	S	U	U	Blue
$\mathcal{J}_{25} = (8, 14^2 7)$	U		U		U	S	Orange
$\mathcal{J}_{26} = (8, 17)$	U				U	S	Orange
$\mathcal{J}_{27} = (7, 1)$	U				S		Olive
$\mathcal{J}_{28} = (7, 14^1 4^2)$	U	U	U		S		Olive
$\mathcal{J}_{29} = (8, 14^1 4^2 7)$	U	U	U		U	S	Orange
$\mathcal{J}_{30} = (7, 14^1 4^2 6)$	U	U	U	U	S		Olive
$\mathcal{J}_{31} = (., 14^2 67)$	U		U	U	U		Cyan
$\mathcal{J}_{32} = (., 14^2 678)$	U		U	U	U	U	RosyBrown

$\mathcal{J}_5, \mathcal{J}_{30}, \mathcal{J}_{31}$ and $\mathcal{J}_{32}$ of instability of SS6. Indeed, crossing the surfaces Γ_3 and Γ_4 from $\mathcal{J}_3$ to $\mathcal{J}_5$ or from $\mathcal{J}_{22}$ to $\mathcal{J}_{30}$ or from $\mathcal{J}_{23}$ to $\mathcal{J}_{31}$ or from $\mathcal{J}_{24}$ to $\mathcal{J}_{32}$ in the cases without and with mortality, respectively, the positive steady state SS6 losses its stability via a Hopf bifurcation with emergence of a stable limit cycle (see Table 3 and Figs. 4 and 5). Notice that, in the case with maintenance and for D fixed, the value of $S_{\text{ch}}^{\text{in}}$ at which SS6 losses its stability, is larger than that in the case without maintenance. Moreover, the new regions $\mathcal{J}_{31}$ and $\mathcal{J}_{32}$ appear under the influence of the maintenance terms.

3.1.4. *Hydrogen and phenol are added in the input.* In the following, we study the operating diagrams of system (1) in the $\left(S_{\text{ch}}^{\text{in}}, D\right)$-plane by assuming that $S_{\text{ph}}^{\text{in}} = 1$ and $S_{\text{H}_2}^{\text{in}} = 2.67 \times 10^{-2}$ as in Fig. 5(d) of [30]. Figs. 6(a) and 7(a) represent the operating diagrams in the $\left(S_{\text{ch}}^{\text{in}}, D\right)$-plane, in the cases without and with maintenance, respectively. The magnifications shown in Fig. 6(b)–(f) put in evidence the regions $\mathcal{J}_i$, $i = 16, 17, 33, \ldots, 44$. Fig. 7 shows that the regions $\mathcal{J}_i$, $i = 1, 6, \ldots, 10, 16, 17, 33, \ldots, 38$ are similar to those in Fig. 6. We see also that the maintenance has an effect on the disappearance of regions $\mathcal{J}_i$, $i = 39, \ldots, 44$. Moreover, the addition of both the phenol and hydrogen input concentrations to the system contribute to the emergence of twelve new regions $\mathcal{J}_i$, $i = 33, \ldots, 44$, which do not exist with only phenol addition. The existence and the stability of the steady states of (1) in the twenty regions $\mathcal{J}_i$, $i = 1, 6, \ldots, 10, 16, 17, 33, \ldots, 44$, in the operating diagrams of Figs. 6 and 7 are summarized in Table 4. Since the concentrations of $S_{\text{ph}}^{\text{in}}$ and $S_{\text{H}_2}^{\text{in}}$ are large enough comparing with the case of Fig. 5 where $S_{\text{ph}}^{\text{in}} = 10^{-2}$ and $S_{\text{H}_2}^{\text{in}} = 0$, all asymptotic behaviors were detected in Fig. 5(d) of [30].

3.2. **Operating diagrams in the $\left(S_{\text{H}_2}^{\text{in}}, S_{\text{ph}}^{\text{in}}\right)$ plane when D and $S_{\text{ch}}^{\text{in}}$ are fixed.** Now, let D and $S_{\text{ch}}^{\text{in}}$ be fixed. Then, the intersections of the surfaces Γ_i, $i = 3, 4, 8, 9, 11, 12, 13, 15$ with the $\left(S_{\text{H}_2}^{\text{in}}, S_{\text{ph}}^{\text{in}}\right)$ plane are curves of functions of $S_{\text{H}_2}^{\text{in}}$.

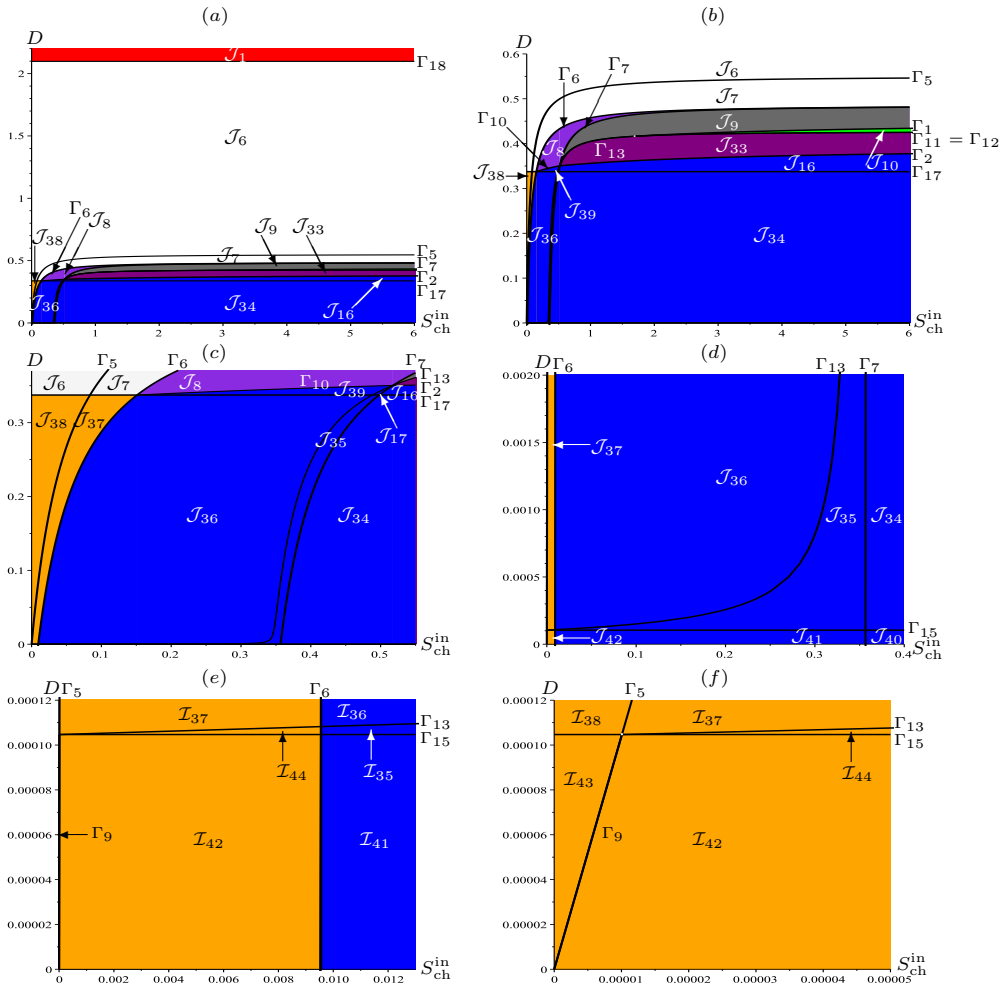

FIGURE 6. Operating diagram in the plane $\left(S^{in}_{ch}, D\right)$, when $S^{in}_{ph} = 1$, $S^{in}_{H_2} = 2.67 \times 10^{-2}$ and $k_{dec,i} = 0$. Magnifications (b) for $D \in [0, 0.6]$ showing the regions $\mathcal{J}_{10}$ and $\mathcal{J}_{39}$, (c) for $D \in [0, 0.37]$ showing the regions $\mathcal{J}_{17}$, $\mathcal{J}_{35}$ and $\mathcal{J}_{37}$, (d) for $D \in [0, 0.002]$ showing the regions $\mathcal{J}_{40}$, $\mathcal{J}_{41}$ and $\mathcal{J}_{42}$, (e) for $D \in [0, 0.00012]$ showing the region $\mathcal{J}_{44}$, (f) for $S^{in}_{ch} \in [0, 0.00005]$ showing the region $\mathcal{J}_{43}$.

However, the intersections of the surfaces Γ_j, $j = 1, 2, 5, 7, 10, 14, 16, 17, 18$ with the plane $\left(S^{in}_{H_2}, S^{in}_{ph}\right)$ are straight lines. We consider the input concentration $S^{in}_{ch} = 0.5$ and $D = 0.25$. These values are those of Fig. 6(a) in [30]. The operating diagrams in the plane $\left(S^{in}_{H_2}, S^{in}_{ph}\right)$ are shown in Figs. 8 and 9, in both cases without and with considering maintenance, respectively. The magnification shown in Fig. 8(b) puts in evidence the regions $\mathcal{J}_i$, $i = 2, 3, 22, 23, 24, 40, 45, \ldots, 49$. The magnification presented in Fig. 9(b) shows the regions $\mathcal{J}_i$, $i = 1, 2, 3, 22, 23, 24, 40, 45, \ldots, 51$. The existence and the stability of the steady states of (1) in the twenty-four regions $\mathcal{J}_i$, of the operating diagrams of Figs. 8 and 9 are summarized in Table 5.

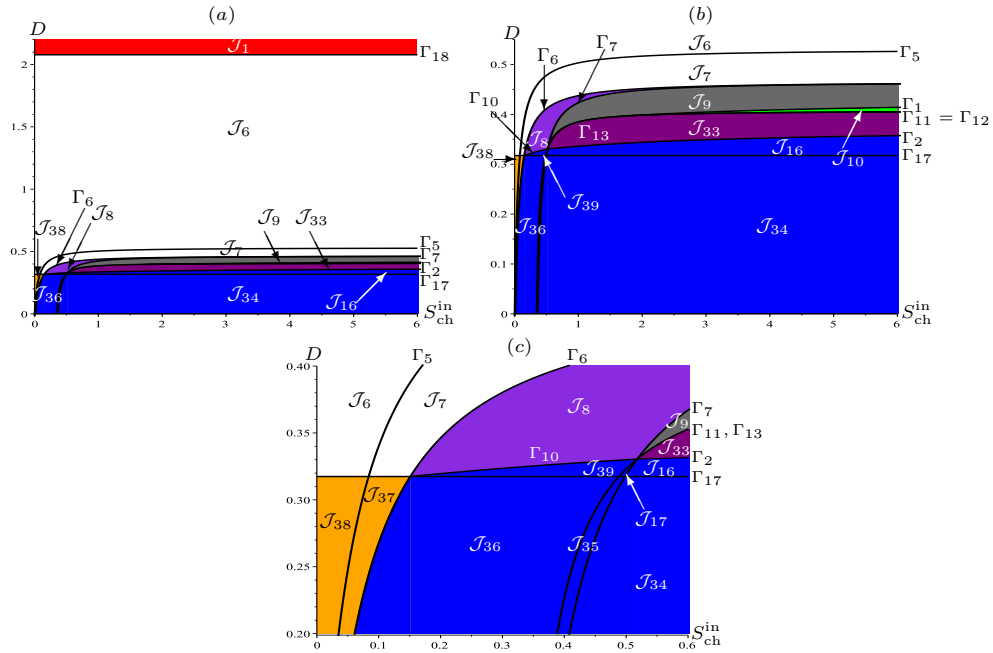

FIGURE 7. Operating diagram in the plane $\left(S^{in}_{ch}, D\right)$, when $S^{in}_{ph} = 1$, $S^{in}_{H_2} = 2.67 \times 10^{-2}$ and $k_{dec,i} > 0$. Magnifications (b) for $D \in [0, 0.55]$ showing the regions $\mathcal{J}_{10}$ and $\mathcal{J}_{39}$, (c) for $D \in [0.2, 0.4]$ showing the regions $\mathcal{J}_{17}$, $\mathcal{J}_{35}$ and $\mathcal{J}_{37}$.

TABLE 4. Existence and local stability of steady states in the regions of the operating diagrams of Figs. 6 and 7.

Region	SS1	SS2	SS3	SS4[1]	SS4[2]	SS5	SS6	SS7	SS8	Color
$\mathcal{J}_1 = (1)$	S									Red
$\mathcal{J}_6 = (2, 1)$	U	S								White
$\mathcal{J}_7 = (2, 13)$	U	S	U							White
$\mathcal{J}_8 = (5, 123)$	U	U	U			S				Blueviolet
$\mathcal{J}_9 = (3, 12)$	U	U	S							DimGray
$\mathcal{J}_{10} = (34^2, 124^1)$	U	U	S	U	S					Green
$\mathcal{J}_{16} = (6, 1234^2)$	U	U	U		U		S			Blue
$\mathcal{J}_{17} = (6, 1234^2 5)$	U	U	U		U	U	S			Blue
$\mathcal{J}_{33} = (4^2, 123)$	U	U	U		S					Purple
$\mathcal{J}_{34} = (6, 1234^2 8)$	U	U	U		U		S		U	Blue
$\mathcal{J}_{35} = (6, 1234^2 58)$	U	U	U		U	U	S		U	Blue
$\mathcal{J}_{36} = (6, 12358)$	U	U	U			U	S		U	Blue
$\mathcal{J}_{37} = (8, 123)$	U	U	U						S	Orange
$\mathcal{J}_{38} = (8, 12)$	U	U							S	Orange
$\mathcal{J}_{39} = (6, 1235)$	U	U	U			U	S			Blue
$\mathcal{J}_{40} = (6, 1234^2 78)$	U	U	U		U		S	U	U	Blue
$\mathcal{J}_{41} = (6, 1234^2 578)$	U	U	U		U	U	S	U	U	Blue
$\mathcal{J}_{42} = (8, 1234^2 7)$	U	U	U		U			U	S	Orange
$\mathcal{J}_{43} = (8, 127)$	U	U						U	S	Orange
$\mathcal{J}_{44} = (8, 1234^2)$	U	U	U		U				S	Orange

From Table 5 and the operating diagrams shown in Figs. 8 and 9, the new regions $\mathcal{J}_1$, $\mathcal{J}_9$, $\mathcal{J}_{33}$, $\mathcal{J}_{50}$ and $\mathcal{J}_{51}$ appear under the influence of the maintenance terms. The

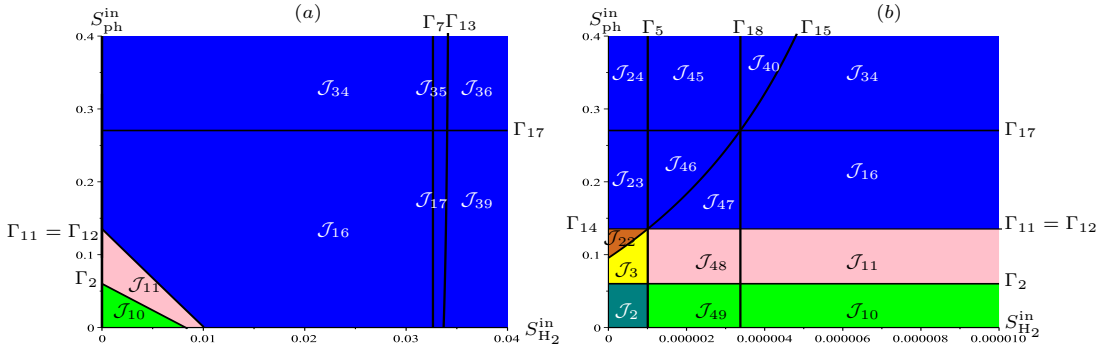

FIGURE 8. Operating diagram in the plane $\left(S^{in}_{H_2}, S^{in}_{ph}\right)$, when $D = 0.25$, $S^{in}_{ch} = 0.5$ and $k_{dec,i} = 0$. Magnification (b) for $S^{in}_{H_2} \in [0, 10^{-5}]$ showing the regions $\mathcal{J}_2$, $\mathcal{J}_3$, $\mathcal{J}_{40}$, $\mathcal{J}_i$, $i = 22, \ldots, 24$ and $\mathcal{J}_j$, $j = 45, \ldots, 49$.

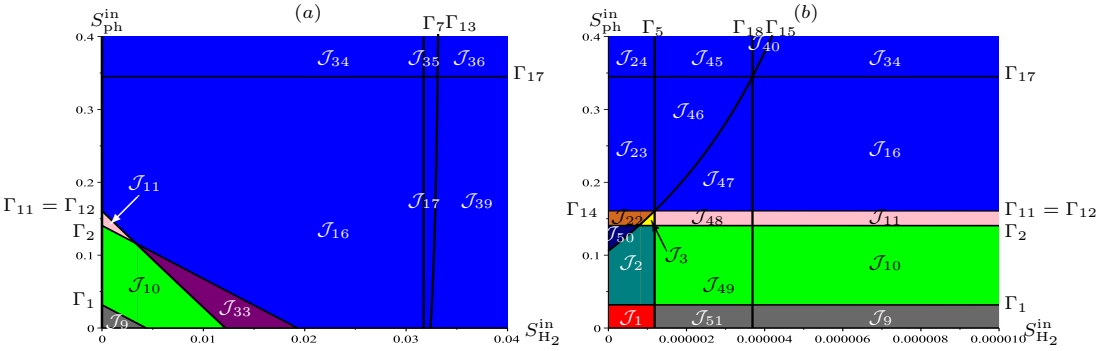

FIGURE 9. Operating diagram in the plane $\left(S^{in}_{H_2}, S^{in}_{ph}\right)$, when $D = 0.25$, $S^{in}_{ch} = 0.5$ and $k_{dec,i} > 0$. Magnification (b) for $S^{in}_{H_2} \in [0, 10^{-5}]$ showing the regions $\mathcal{J}_1$, $\mathcal{J}_2$, $\mathcal{J}_3$, $\mathcal{J}_{40}$, $\mathcal{J}_i$, $i = 22, \ldots, 24$ and $\mathcal{J}_j$, $j = 45, \ldots, 51$.

regions $\mathcal{J}_i$, $i = 1, 3, 9, 11, 22, 48, 50, 51$ are not reported in the numerical operating diagram of Fig. 6(a) of [30] in the case including maintenance.

4. **Conclusion.** In this work, we gave an analytical study of the operating diagrams of the three-tiered food web model (1) developed in [30]. Considering the three input substrate concentrations, as well as the maintenance, we compare our results with those obtained by the numerical method in [30]. Using the mathematical analysis of the existence and the stability of the steady states of model (1) in [20, 21] for a large class of growth functions, we have determined theoretically the operating diagrams to provide a complete description of the dynamical behavior of the process, according to the control parameters S^{in}_{ch}, S^{in}_{ph}, $S^{in}_{H_2}$ and D.

For $S^{in}_{ph} = S^{in}_{H_2} = 0$, the operating diagrams in the $\left(S^{in}_{ch}, D\right)$ plane of Fig. 1 show the same number of regions in both cases with and without maintenance, with variations only in their shape and extension. In the case of maintenance, our analytical study of the operating diagrams confirmes the numerical results of [26] where a stable limit cycle bifurcates from the positive steady state via a Hopf

TABLE 5. Existence and local stability of steady states in the regions of the operating diagrams of Figs. 8 and 9.

Region	SS1	SS2	SS3	$SS4^1$	$SS4^2$	SS5	SS6	SS7	SS8	Color
$\mathcal{J}_1 = (1)$	S									Red
$\mathcal{J}_2 = (14^2, 4^1)$	S			U	S					Teal
$\mathcal{J}_3 = (16, 4^1 4^2)$	S			U	U		S			Yellow
$\mathcal{J}_9 = (3, 12)$	U	U	S							DimGray
$\mathcal{J}_{10} = (34^2, 124^1)$	U	U	S	U	S					Green
$\mathcal{J}_{11} = (36, 124^1 4^2)$	U	U	S	U	U		S			Pink
$\mathcal{J}_{16} = (6, 1234^2)$	U	U	U		U		S			Blue
$\mathcal{J}_{17} = (6, 1234^2 5)$	U	U	U		U	U	S			Blue
$\mathcal{J}_{22} = (67, 14^1 4^2)$	U			U	U		S	S		Chocolate
$\mathcal{J}_{23} = (6, 14^2 7)$	U				U		S	U		Blue
$\mathcal{J}_{24} = (6, 14^2 78)$	U				U		S	U	U	Blue
$\mathcal{J}_{33} = (4^2, 123)$	U	U	U		S					Purple
$\mathcal{J}_{34} = (6, 1234^2 8)$	U	U	U		U		S		U	Blue
$\mathcal{J}_{35} = (6, 1234^2 58)$	U	U	U		U	U	S		U	Blue
$\mathcal{J}_{36} = (6, 12358)$	U	U	U			U	S		U	Blue
$\mathcal{J}_{39} = (6, 1235)$	U	U	U			U	S			Blue
$\mathcal{J}_{40} = (6, 1234^2 78)$	U	U	U		U		S	U	U	Blue
$\mathcal{J}_{45} = (6, 134^2 78)$	U		U		U		S	U	U	Blue
$\mathcal{J}_{46} = (6, 134^2 7)$	U		U		U		S	U		Blue
$\mathcal{J}_{47} = (6, 134^2)$	U		U		U		S			Blue
$\mathcal{J}_{48} = (36, 14^1 4^2)$	U		S	U	U		S			Pink
$\mathcal{J}_{49} = (34^2, 14^1)$	U		S	U	S					Green
$\mathcal{J}_{50} = (4^2 7, 14^1)$	U			U	S			S		Navy
$\mathcal{J}_{51} = (3, 1)$	U		S							DimGray

bifurcation. Indeed, this behavior is unreported in the numerical operating diagram of Fig. 2 in [30].

Considering the inflowing concentrations $S_{\text{ph}}^{\text{in}} = 0$ and $S_{\text{H}_2}^{\text{in}} = 2.67 \times 10^{-5}$ of Fig. 3(a) in [30], Fig. 2 shows the destabilization of the positive steady state in the case without maintenance. In the regions $\mathcal{J}_{20}$ and $\mathcal{J}_{21}$, all the steady states are unstable so that there is coexistence around a limit cycle for any positive initial conditions. Adding the maintenance, the regions $\mathcal{J}_i$, $i = 14, \ldots, 21$ disappear. In addition, Fig. 3 shows that the regions $\mathcal{J}_8$ (stability of SS5) and $\mathcal{J}_{13}$ (stability of SS3 with instability of SS6) have been omitted. Crossing $\mathcal{J}_{11}$ to $\mathcal{J}_{13}$, there is bistability of SS3 and a limit cycle. In the regions $\mathcal{J}_8$ and $\mathcal{J}_{13}$, the outcome of the process is different than that found in the numerical operating diagram in [30].

Similarly, for the input concentrations $S_{\text{ph}}^{\text{in}} = 10^{-2}$ and $S_{\text{H}_2}^{\text{in}} = 0$ in Fig. 5(a) of [30], Figs. 4 and 5 prove that the region $\mathcal{J}_{22}$ (bistability of SS6 and SS7), and the regions $\mathcal{J}_5, \mathcal{J}_{30}, \mathcal{J}_{31}$ and $\mathcal{J}_{32}$ (instability of SS6) were not been detected.

However, when the input concentrations $S_{\text{ph}}^{\text{in}} = 1$ and $S_{\text{H}_2}^{\text{in}} = 2.67 \times 10^{-2}$ are large enough as in Fig. 5(d) of [30], our analytical operating diagrams in Figs. 6 and 7 show that all asymptotic behaviors were detected.

Finally, when $S_{\text{ch}}^{\text{in}} = 0.5$ and $D = 0.25$ are fixed as in Fig. 6(a) of [30], our operating diagrams in $\left(S_{\text{H}_2}^{\text{in}}, S_{\text{ph}}^{\text{in}}\right)$ plane of Figs. 8 and 9 prove that the regions $\mathcal{J}_i$, $i = 1, 3, 9, 11, 22, 48, 50, 51$ are unreported. In fact, there can be stability of only SS1 ($i = 1$) or SS3 ($i = 9, 51$), or bistability of SS1 and SS6 ($i = 3$) or of SS3 and SS6 ($i = 11, 48$) or of SS6 and SS7 ($i = 22$) or of SS4 and SS7 ($i = 50$).

Thus, our mathematical study of the operating diagram of the three-tiered food web model (1) shows the omission of several fairly important asymptotic behaviors in the numerical study of [30]. Especially validated models with realistic parametrization from experimental data, more attention should be paid to numerical resolution. However, the theoretical study of the operating diagram remains the only way to ensure the accuracy of the results. Moreover, our results allow us to answer the delicate question: the maintenance does not destabilize the steady states but modifies the shape of the regions. It has also an effect on the appearance and the disappearance of some regions.

Appendix A. **Mathematical analysis of the model.** In this section, we recall from [20, 21] the main results of existence and stability of all steady states of system (1). Following [26], we can rescale model (1) to reduce the number of yield parameters and ease the mathematical analysis. We use the following change of variables:

$$x_0 = \tfrac{Y}{Y_0} X_{\rm ch}, x_1 = \tfrac{Y_4}{Y_1} X_{\rm ph}, x_2 = \tfrac{1}{Y_2} X_{\rm H_2}, s_0 = Y S_{\rm ch}, s_1 = Y_4 S_{\rm ph}, s_2 = S_{\rm H_2}, \tag{3}$$

where the yield coefficients are

$$Y_0 = Y_{\rm ch},\ Y_1 = Y_{\rm ph},\ Y_2 = Y_{\rm H_2},\ Y_3 = \frac{224}{208}(1 - Y_0),\ Y_4 = \frac{32}{224}(1 - Y_1),$$

with $Y = Y_3 Y_4$ and $\omega = \frac{16}{208 Y}$. The inflowing concentrations are:

$$s_0^{\rm in} = Y S_{\rm ch}^{\rm in}, \quad s_1^{\rm in} = Y_4 S_{\rm ph}^{\rm in}, \quad s_2^{\rm in} = S_{\rm H_2}^{\rm in}, \tag{4}$$

the death rates are $a_0 = k_{\rm dec,ch}$, $a_1 = k_{\rm dec,ph}$ and $a_2 = k_{\rm dec,H_2}$. Under the scaling (3), the growth functions become:

$$\mu_0(s_0, s_2) = \tfrac{m_0 s_0}{K_0 + s_0} \tfrac{s_2}{L_0 + s_2}, \quad \mu_1(s_1, s_2) = \tfrac{m_1 s_1}{K_1 + s_1} \tfrac{1}{1 + s_2/K_I}, \quad \mu_2(s_2) = \tfrac{m_2 s_2}{K_2 + s_2}, \tag{5}$$

where

$$\begin{aligned} &m_0 = Y_0 k_{m,\rm ch}, \quad K_0 = Y K_{S,\rm ch}, \quad L_0 = K_{S,\rm H_2,c}, \quad m_1 = Y_1 k_{m,\rm ph}, \\ &K_1 = Y_4 K_{S,\rm ph}, \quad K_I = K_{I,\rm H_2}, \quad m_2 = Y_2 k_{m,\rm H_2}, \quad K_2 = K_{S,\rm H_2}. \end{aligned}$$

Using the change of variables (3) and (4), and Table 2 in [21], we can recall now the steady states of system (1) in Table 6. From Table 3 in [20] and the change of variables (4), all necessary and sufficient existence and stability conditions of the steady states of (1) in the case with maintenance are stated in Table 7.

Remark 3. In the case without maintenance, the necessary and sufficient conditions of existence and local stability can be deduced from Table 7 by taking $a_i = 0$, except for the stability condition of SS6 which is given by

$$\phi_3(D) \geq 0, \quad \text{or} \quad \phi_3(D) < 0 \quad \text{and} \quad \phi_4(D, S_{\rm ch}^{\rm in}, S_{\rm ph}^{\rm in}, S_{\rm H_2}^{\rm in}) > 0, \tag{6}$$

where the function ϕ_3 is defined in Table 1 in [21] and ϕ_4 is defined by:

$$\begin{aligned} \phi_4(D, S_{\rm ch}^{\rm in}, S_{\rm ph}^{\rm in}, S_{\rm H_2}^{\rm in}) \ = \ & (EIx_0x_2 + EG\phi_3(D)x_0x_1)(Ix_2 + (G+H)x_1 \\ & + (E + \omega F)x_0) + (Ix_2 + (G+H)x_1 + \omega F x_0) GI x_1 x_2, \end{aligned} \tag{7}$$

with

$$E = \tfrac{\partial \mu_0}{\partial s_0}(s_0, s_2),\ F = \tfrac{\partial \mu_0}{\partial s_2}(s_0, s_2),\ G = \tfrac{\partial \mu_1}{\partial s_1}(s_1, s_2),\ H = -\tfrac{\partial \mu_1}{\partial s_2}(s_1, s_2),\ I = \tfrac{d\mu_2}{ds_2}(s_2).$$

TABLE 6. The steady states of (1). The function μ_i are given by (5). The function M_i, ψ_i and Ψ are given in Table 11 in [21]. For the general case, the functions are given in Table 1 in [21].

	s_0, s_1, s_2	x_0, x_1, x_2
SS1	$s_0 = Y S^{in}_{ch}$, $s_1 = Y_4 S^{in}_{ph}$, $s_2 = S^{in}_{H_2}$	$x_0 = 0$, $x_1 = 0$, $x_2 = 0$
SS2	$s_0 = Y S^{in}_{ch}$, $s_1 = Y_4 S^{in}_{ph}$, $s_2 = M_2(D + a_2)$	$x_0 = 0$, $x_1 = 0$, $x_2 = \frac{D}{D+a_2}\left(S^{in}_{H_2} - s_2\right)$
SS3	$s_0 = s_0\left(D, S^{in}_{ch}, S^{in}_{H_2}\right)$ is a solution of $\psi_0(s_0) = D + a_0$, $s_1 = Y_4 S^{in}_{ph} + Y S^{in}_{ch} - s_0$, $s_2 = S^{in}_{H_2} - \omega\left(Y S^{in}_{ch} - s_0\right)$	$x_0 = \frac{D}{D+a_0}\left(Y S^{in}_{ch} - s_0\right)$, $x_1 = 0$, $x_2 = 0$
SS4	$s_2 = s_2\left(D, S^{in}_{ch}, S^{in}_{ph}, S^{in}_{H_2}\right)$ is a solution of $\Psi(s_2, D) = (1-\omega) Y S^{in}_{ch} + Y_4 S^{in}_{ph} + S^{in}_{H_2}$, $s_0 = M_0(D + a_0, s_2)$, $s_1 = M_1(D + a_1, s_2)$	$x_0 = \frac{D}{D+a_0}\left(Y S^{in}_{ch} - s_0\right)$, $x_1 = \frac{D}{D+a_1}\left(Y S^{in}_{ch} + Y_4 S^{in}_{ph} - s_0 - s_1\right)$, $x_2 = 0$
SS5	$s_0 = M_0(D + a_0, M_2(D + a_2))$, $s_1 = Y S^{in}_{ch} + Y_4 S^{in}_{ph} - s_0$, $s_2 = M_2(D + a_2)$	$x_0 = \frac{D}{D+a_0}\left(Y S^{in}_{ch} - s_0\right)$, $x_1 = 0$, $x_2 = \frac{D}{D+a_2}\left(S^{in}_{H_2} - s_2 - \omega\left(Y S^{in}_{ch} - s_0\right)\right)$
SS6	$s_0 = M_0(D + a_0, M_2(D + a_2))$, $s_1 = M_1(D + a_1, M_2(D + a_2))$, $s_2 = M_2(D + a_2)$	$x_0 = \frac{D}{D+a_0}\left(Y S^{in}_{ch} - s_0\right)$, $x_2 = \frac{D}{D+a_2}\left((1-\omega)\left(Y S^{in}_{ch} - s_0\right) + Y_4 S^{in}_{ph} + S^{in}_{H_2} - s_1 - s_2\right)$, $x_1 = \frac{D}{D+a_1}\left(Y S^{in}_{ch} + Y_4 S^{in}_{ph} - s_0 - s_1\right)$
SS7	$s_0 = Y S^{in}_{ch}$, $s_1 = s_1\left(D, S^{in}_{ph}, S^{in}_{H_2}\right)$ is a solution of $\psi_1(s_1) = D + a_1$, $s_2 = Y_4 S^{in}_{ph} + S^{in}_{H_2} - s_1$	$x_0 = 0$, $x_1 = \frac{D}{D+a_1}\left(Y_4 S^{in}_{ph} - s_1\right)$, $x_2 = 0$
SS8	$s_0 = Y S^{in}_{ch}$, $s_1 = M_1(D + a_1, M_2(D + a_2))$, $s_2 = M_2(D + a_2)$	$x_0 = 0$, $x_1 = \frac{D}{D+a_1}\left(Y_4 S^{in}_{ph} - s_1\right)$, $x_2 = \frac{D}{D+a_2}\left(Y_4 S^{in}_{ph} + S^{in}_{H_2} - s_1 - s_2\right)$

Appendix B. **Proof of the operating diagrams in Fig. 1.** In this section, we present the method used to construct theoretically the operating diagrams presented in Fig. 1. To this end, we plot the various curves from the existence and stability conditions which depend on the operating parameters. In addition, we will see in the following that the proof is supported by numerical experimentation when the biological parameter values are fixed and $S^{in}_{ph} = S^{in}_{H_2} = 0$. In this case, it is easy to see from Table 7 that only the three steady states SS1, SS4 and SS6 exist. In the case with or without maintenance ($a_i = 0$), SS1 always exists and it is stable, since all stability conditions in Table 7 hold, as

$$\mu_0\left(S^{in}_{ch} Y, S^{in}_{H_2}\right) = \mu_1\left(S^{in}_{ph} Y_4, S^{in}_{H_2}\right) = \mu_2\left(S^{in}_{H_2}\right) = 0 < D + a_i.$$

From Proposition 2 in [21], SS4 and SS6 exist, respectively, if and only if

$$(1-\omega) S^{in}_{ch} Y \geq \phi_1(D) \quad \text{and} \quad (1-\omega) S^{in}_{ch} Y > \phi_2(D). \tag{8}$$

Recall first the surfaces Γ_i, $i = 1, \ldots, 18$ defined in Table 9. From the first condition of (8), SS4 exists in the region bounded by the curve Γ_1 and located at the right of this curve, see Figs. 10 and 13. From Remark 3.2 of [20], when it exists, $SS4^1$ is unstable and the second stability condition of $SS4^2$ in Table 7 is always satisfied. The first stability condition of $SS4^2$ holds for all $\left(S^{in}_{ch}, D\right)$ in the region bounded by the curve Γ_2 and located at the left of this curve. The third stability condition of $SS4^2$ holds for all $D > \overline{D}$, where $\overline{D}$ is the unique solution of $\phi_3(D) = 0$, see Fig. 11(a). Numerical computations show that the curves Γ_1 and Γ_2 are tangent for $D = \overline{D}$ and $\phi_1(D) < \phi_2(D)$, for all D in their definition domains. Then, $SS4^2$ is stable in the region located between the two curves Γ_1 and Γ_2 and above the line

TABLE 7. Case of maintenance: necessary and sufficient existence and local stability conditions of steady states of (1). The functions c_3, c_5, r_3 and r_5, used in the stability condition of SS6, are given in Table 2 in [20]. All other functions are given in Table 8 of [20].

	Existence conditions	Stability conditions
SS1	always exists	$\mu_0\left(S^{\rm in}_{\rm ch}Y, S^{\rm in}_{\rm H_2}\right) < D + a_0$, $\mu_1\left(S^{\rm in}_{\rm ph}Y_4, S^{\rm in}_{\rm H_2}\right) < D + a_1$, $\mu_2\left(S^{\rm in}_{\rm H_2}\right) < D + a_2$
SS2	$\mu_2\left(S^{\rm in}_{\rm H_2}\right) > D + a_2$	$S^{\rm in}_{\rm ch}Y < \varphi_0(D)$, $S^{\rm in}_{\rm ph}Y_4 < \varphi_1(D)$
SS3	$\mu_0\left(S^{\rm in}_{\rm ch}Y, S^{\rm in}_{\rm H_2}\right) > D + a_0$	$\mu_1\left(S^{\rm in}_{\rm ch}Y + S^{\rm in}_{\rm ph}Y_4 - s_0, S^{\rm in}_{\rm H_2} - \omega\left(S^{\rm in}_{\rm ch}Y - s_0\right)\right) < D + a_1$ $S^{\rm in}_{\rm H_2} - \omega S^{\rm in}_{\rm ch}Y < M_2(D + a_2) - \omega\varphi_0(D)$ with s_0 solution of equation $\psi_0(s_0) = D + a_0$
SS4	$(1-\omega)S^{\rm in}_{\rm ch}Y + S^{\rm in}_{\rm ph}Y_4 + S^{\rm in}_{\rm H_2} \geq \phi_1(D)$, $S^{\rm in}_{\rm ch}Y > M_0\left(D + a_0, s_2\right)$, $S^{\rm in}_{\rm ch}Y + S^{\rm in}_{\rm ph}Y_4 > M_0\left(D + a_0, s_2\right) + M_1\left(D + a_1, s_2\right)$, with s_2 solution of equation $\Psi(s_2) = (1-\omega)S^{\rm in}_{\rm ch}Y + S^{\rm in}_{\rm ph}Y_4 + S^{\rm in}_{\rm H_2}$	$(1-\omega)S^{\rm in}_{\rm ch}Y + S^{\rm in}_{\rm ph}Y_4 + S^{\rm in}_{\rm H_2} < \phi_2(D)$, $\dfrac{\partial\Psi}{\partial s_2}(s_2, D) > 0$ and $\phi_3(D) > 0$
SS5	$S^{\rm in}_{\rm ch}Y > \varphi_0(D)$, $S^{\rm in}_{\rm H_2} - \omega S^{\rm in}_{\rm ch}Y > M_2(D + a_2) - \omega\varphi_0$	$S^{\rm in}_{\rm ch}Y + S^{\rm in}_{\rm ph}Y_4 < \varphi_0(D) + \varphi_1(D)$
SS6	$(1-\omega)S^{\rm in}_{\rm ch}Y + S^{\rm in}_{\rm ph}Y_4 + S^{\rm in}_{\rm H_2} > \phi_2(D)$, $S^{\rm in}_{\rm ch}Y > \varphi_0(D)$, $S^{\rm in}_{\rm ch}Y + S^{\rm in}_{\rm ph}Y_4 > \varphi_0(D) + \varphi_1(D)$	$c_3 > 0$, $c_5 > 0$, $r_4 > 0$, $r_5 > 0$
SS7	$\mu_1\left(S^{\rm in}_{\rm ph}Y_4, S^{\rm in}_{\rm H_2}\right) > D + a_1$	$S^{\rm in}_{\rm ph}Y_4 + S^{\rm in}_{\rm H_2} < M_1\left(D + a_1, M_3\left(S^{\rm in}_{\rm ch}Y, D + a_0\right)\right) + M_3\left(S^{\rm in}_{\rm ch}Y, D + a_0\right)$, $S^{\rm in}_{\rm ph}Y_4 + S^{\rm in}_{\rm H_2} < \varphi_1(D) + M_2(D + a_2)$
SS8	$S^{\rm in}_{\rm ph}Y_4 > \varphi_1(D)$, $S^{\rm in}_{\rm ph}Y_4 + S^{\rm in}_{\rm H_2} > \varphi_1(D) + M_2(D + a_2)$	$S^{\rm in}_{\rm ch}Y < \varphi_0(D)$

$D = \overline{D}$. From the second condition of (8), SS6 exists in the region bounded by the curve Γ_2 and located at the right of this curve, see Figs. 10 and 13.

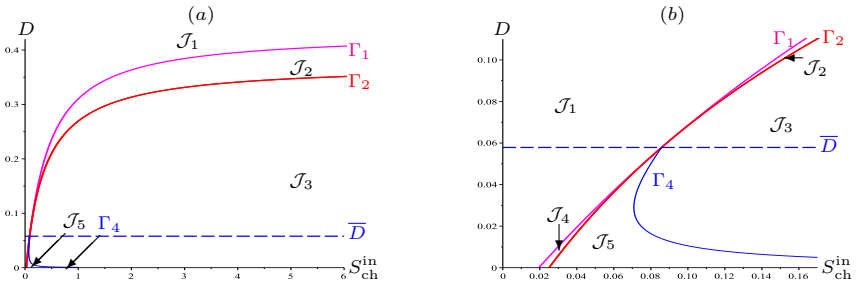

FIGURE 10. With maintenance: (a) curves Γ_1, Γ_2 and Γ_4 and the line $D = \overline{D}$. (b) Magnification for $D \in [0, 0.11]$ showing the region $\mathcal{J}_4$.

B.1. **Case of maintenance.** To determine the regions of stability of SS6 in the case of maintenance, we must establish the signs of the various stability conditions given in Table 7 by

$$c_3(D, S^{\rm in}_{\rm ch}) > 0, \quad c_5(D, S^{\rm in}_{\rm ch}) > 0, \quad r_4(D, S^{\rm in}_{\rm ch}) > 0 \quad \text{and} \quad r_5(D, S^{\rm in}_{\rm ch}) > 0. \tag{9}$$

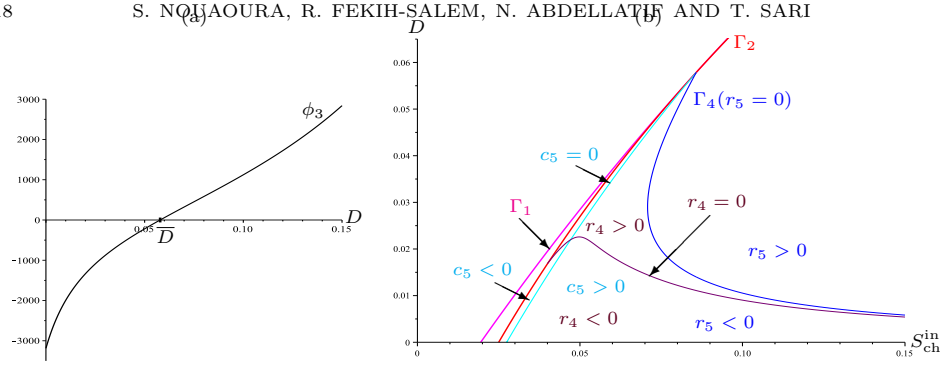

FIGURE 11. With maintenance: (a) curve of the function ϕ_3. (b) Signs of c_5, r_4 and r_5 according to different regions.

To this end, we plot in Fig. 12 the functions c_3, c_5, r_4 and r_5 for different fixed values of D such that

$$S_{ch}^{in} > \sigma(D) := \phi_2(D)/(1-\omega)Y,$$

that is, from the existence condition of SS6. Fig. 12(a) illustrates that the function $c_3(D, S_{ch}^{in})$ is positive for various values of D from the starting points in red of abscissa $\sigma(D)$. Fig. 12(b)–(d) shows the signs of the functions c_3, c_5, r_4 and r_5, and the solutions (green points) of the equations

$$c_5(D, S_{ch}^{in}) = 0, \quad r_4(D, S_{ch}^{in}) = 0 \quad \text{and} \quad r_5(D, S_{ch}^{in}) = 0, \tag{10}$$

for various values of D. Then, solving the set of equations (10) in Maple [18], we

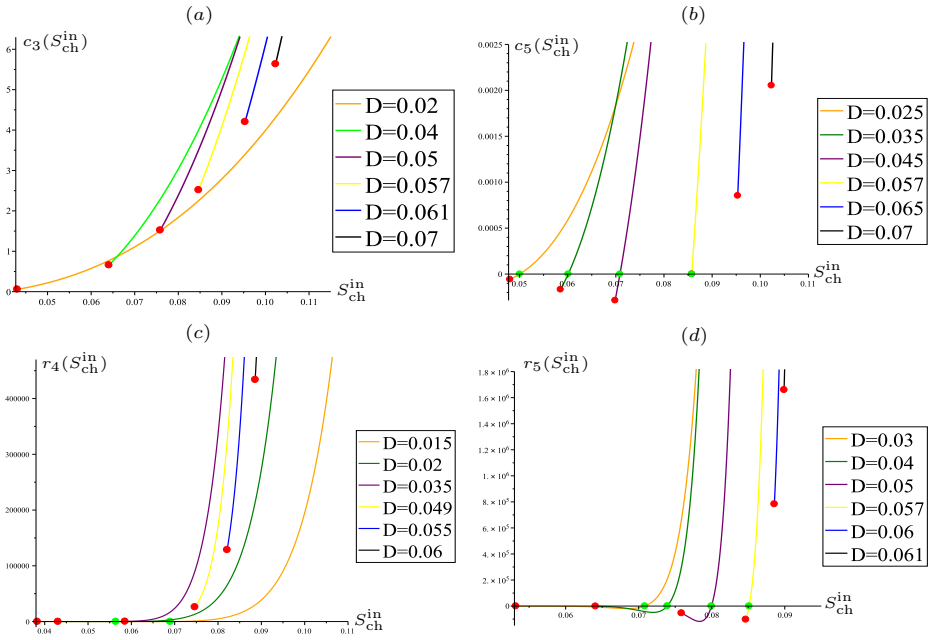

FIGURE 12. With maintenance: curves of the functions c_3, c_5, r_4 and r_5, for $S_{ch}^{in} > \sigma(D)$ (in red) for various values of D, showing the solutions in green of the set of equations (10).

construct the corresponding curves in the operating diagram of Fig. 11(b). From

the results in Fig. 12, we deduce the various signs in the region of Fig. 11(b). Hence, all stability conditions of SS6 in (9) hold in the region bounded by the curve Γ_4 and located at the right of this curve, which corresponds to $r_5\left(S_{\rm ch}^{\rm in}, D\right) > 0$. Therefore, SS6 is stable (resp. unstable) in the region $\mathcal{J}_3$ (resp. $\mathcal{J}_5$) located at the right (resp. left) of the curve Γ_4 (see Fig. 10). Table 8 summarizes the various regions in the operating diagrams, according to $S_{\rm ch}^{\rm in}$ and D.

TABLE 8. Case of maintenance: existence and stability of steady states of (1) according to the five regions $\mathcal{J}_i$ of Fig. 1(a).

Condition 1	Condition 2	Region	SS1	SS4^1	SS4^2	SS6
$D > 0$	$(1-\omega)S_{\rm ch}^{\rm in}Y < \phi_1(D)$	$\mathcal{J}_1$	S			
$D \geq \overline{D}$	$\phi_1(D) < (1-\omega)S_{\rm ch}^{\rm in}Y < \phi_2(D)$	$\mathcal{J}_2$	S	U	S	
	$\phi_2(D) < (1-\omega)S_{\rm ch}^{\rm in}Y$	$\mathcal{J}_3$	S	U	U	S
$D < \overline{D}$	$\phi_2(D) < (1-\omega)S_{\rm ch}^{\rm in}Y$ and $r_5 > 0$	$\mathcal{J}_3$	S	U	U	S
	$\phi_1(D) < (1-\omega)S_{\rm ch}^{\rm in}Y < \phi_2(D)$	$\mathcal{J}_4$	S	U	U	
	$\phi_2(D) < (1-\omega)S_{\rm ch}^{\rm in}Y$ and $r_5 < 0$	$\mathcal{J}_5$	S	U	U	U

B.2. **Case without maintenance.** Recall that the stability conditions of SS6 are given by (6) in the case without maintenance. For all $D \geq \overline{D}$, Fig. 14(a) shows that SS6 is stable since $\phi_3(D) \geq 0$. Inversely, when $D < \overline{D}$, we must determine the sign of the function $\phi_4(D, S_{\rm ch}^{\rm in})$. For several values of $D \in [0, \overline{D}[$, Fig. 14 (b) shows the signs of the function $S_{\rm ch}^{\rm in} \mapsto \phi_4(D, S_{\rm ch}^{\rm in})$ and the uniqueness of the solution (green point) of equation $\phi_4(D, S_{\rm ch}^{\rm in}) = 0$. Using Maple [18], we plot the curve Γ_3 of equation $\phi_4(D, S_{\rm ch}^{\rm in}) = 0$. As in the region bounded by the curve Γ_3 and located at the right of this curve, we have $\phi_4(D, S_{\rm ch}^{\rm in}) > 0$, then SS6 is stable in this region (see Fig. 13). The existence and stability of steady states in the five regions of the operating diagram in Fig. 1 (b) can be summarized as in Table 8 by replacing just $r_5 > 0$ by $\phi_4 > 0$.

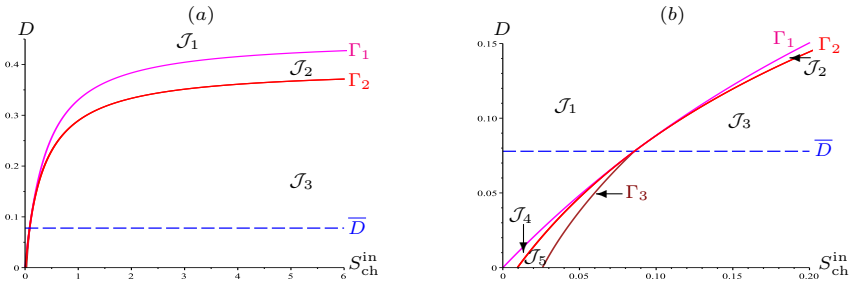

FIGURE 13. Without maintenance: (a) the curves Γ_1, Γ_2 and Γ_3, and the line $D = \overline{D}$. (b) Magnification for $D \in [0, 0.15]$ showing the regions $\mathcal{J}_4$ and $\mathcal{J}_5$.

Appendix C. **Proof of the operating diagram in Fig. 2.** The operating diagram in Fig. 2 considers the case without maintenance when $S_{\rm ph}^{\rm in} = 0$ and $S_{\rm H_2}^{\rm in} = 2.67{\times}10^{-5}$. In the following, the proof is based on the existence and stability conditions of all steady states provided in Table 7 by taking $a_i = 0$, except the stability condition of SS6 given by (6). Thus, SS7 and SS8 do not exist.

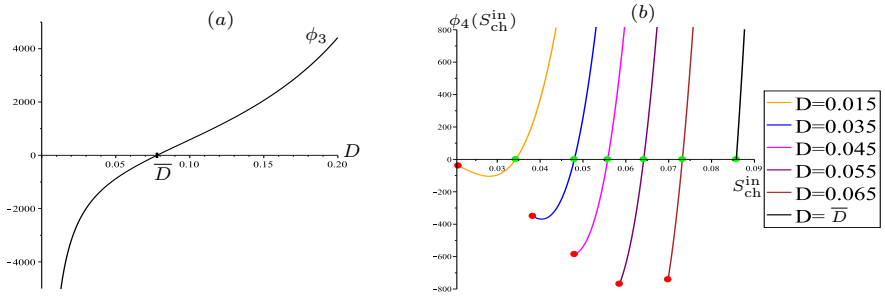

FIGURE 14. Without maintenance: curves of the functions $\phi_3(D)$ (a) and $\phi_4(S_{ch}^{in})$ (b) for $S_{ch}^{in} > \sigma(D)$ (in red) and for several fixed values of D, showing the solution (in green) of $\phi_4(D, S_{ch}^{in}) = 0$.

SS1 always exists and is stable in the region located above the curve Γ_5 and the line Γ_{18}, that is, above the line Γ_{18} (see Fig. 15(a)) since the stability conditions become

$$\mu_0\left(S_{ch}^{in}Y, S_{H_2}^{in}\right) < D, \quad \mu_2\left(S_{H_2}^{in}\right) < D.$$

SS2 exists in the region located below the line Γ_{18}, and it is stable in the region located above the curve Γ_6 (see Fig. 15(a)–(c)) since the existence and stability conditions are (respectively),

$$\mu_2\left(S_{H_2}^{in}\right) > D, \quad S_{ch}^{in}Y < \varphi_0(D).$$

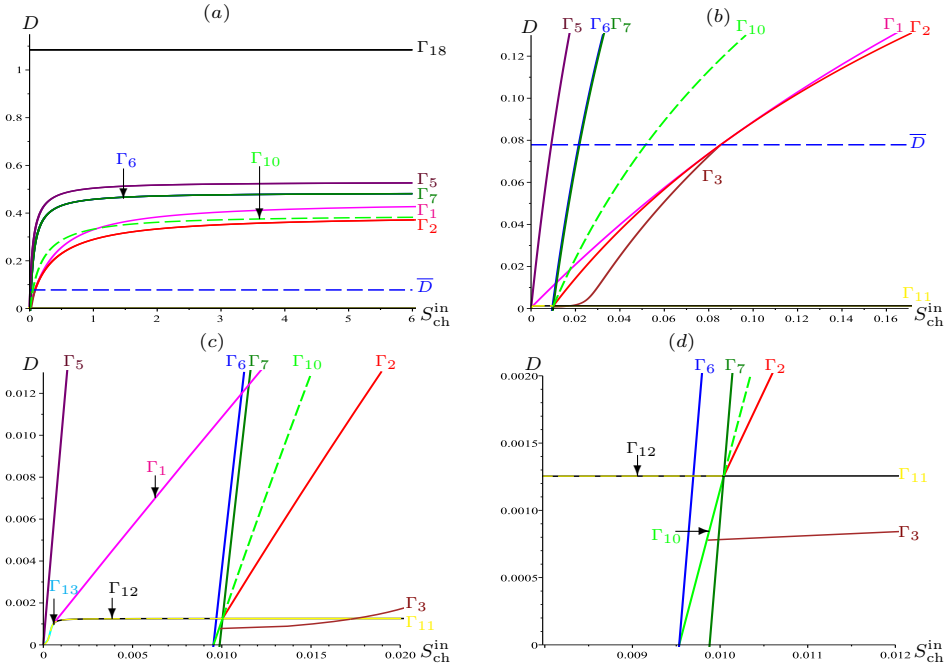

FIGURE 15. (a) All curves of the operating diagram in Fig. 2. Magnification for (b) $D \in [0, 0.13]$, (c) $D \in [0, 0.013]$, (d) $D \in [0, 0.002]$.

SS3 exists in the region located below the curve Γ_5 (see Fig. 15(a)) as the existence condition is

$$\mu_0\left(S_{\rm ch}^{\rm in}Y, S_{\rm H_2}^{\rm in}\right) > D.$$

The stability conditions of SS3 become

$$F(D, S_{\rm ch}^{\rm in}) := \mu_1\left(S_{\rm ch}^{\rm in}Y - s_0, S_{\rm H_2}^{\rm in} - \omega\left(S_{\rm ch}^{\rm in}Y - s_0\right)\right) - D < 0,$$
$$S_{\rm H_2}^{\rm in} - M_2(D) + \omega\varphi_0(D) < \omega S_{\rm ch}^{\rm in}Y.$$

Fig. 16(a) shows that the first stability condition holds in the region located above

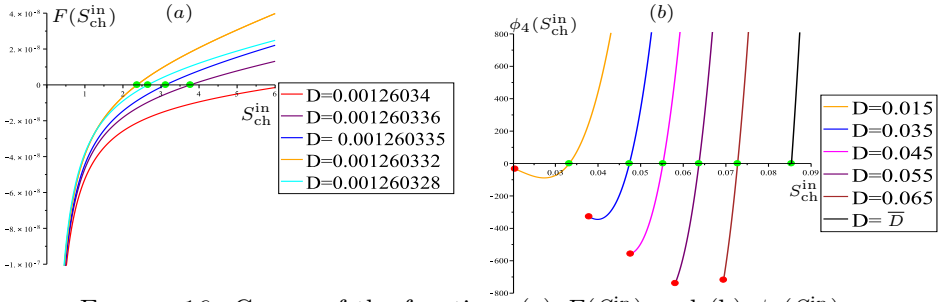

FIGURE 16. Curves of the functions (a) $F(S_{\rm ch}^{\rm in})$ and (b) $\phi_4(S_{\rm ch}^{\rm in})$, for several fixed values of D.

the curve Γ_{11}. Consequently, SS3 is stable in the region located between the two curves Γ_7 and Γ_{11}, see Fig. 15.

For SS4^1 and SS4^2, the existence conditions become

$$(1-\omega)S_{\rm ch}^{\rm in}Y + S_{\rm H_2}^{\rm in} \geq \phi_1(D), \quad G_i(D, S_{\rm ch}^{\rm in}) := S_{\rm ch}^{\rm in}Y - M_0\left(D, s_2^{*i}\right) - M_1\left(D, s_2^{*i}\right) > 0.$$

Hence, the first existence condition holds in the region located at the right of the curve Γ_1, see Fig. 15(a)–(c). Fig. 17 shows that the second existence condition of SS4^1 (resp. SS4^2) holds in the region located at the left (resp. right) of the curve Γ_{12} (resp. Γ_{13}), see Fig. 15(a)–(c).

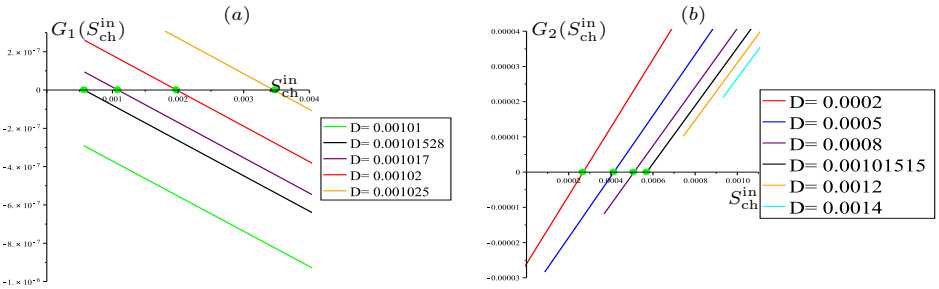

FIGURE 17. Curves of the functions (a) $G_1(S_{\rm ch}^{\rm in})$ and (b) $G_2(S_{\rm ch}^{\rm in})$, for several fixed values of D.

Thus, SS4^1 exists in the region located between the curves Γ_1 and Γ_{12}, while SS4^2 exists in the region located at the right of the curves Γ_1 and Γ_{13}, see Fig. 15(a)–(c). Recall that, SS4^1 is unstable, when it exists, and the stability conditions of SS4^2 become

$$(1-\omega)S_{\rm ch}^{\rm in}Y + S_{\rm H_2}^{\rm in} < \phi_2(D), \quad \phi_3(D) > 0.$$

The first stability condition of SS4^2 holds in the region located at the left of the curve Γ_2. As in Fig. 14(a), the second stability condition holds, for all $D > \overline{D} \simeq 0.078$.

Then, SS4[2] is stable in the region located between the two curves Γ_1 and Γ_2 and above the line $D = \overline{D}$ (see Fig. 15(a)–(b)).

For SS5, the existence conditions become

$$S^{\text{in}}_{\text{ch}} Y > \varphi_0(D), \quad S^{\text{in}}_{\text{H}_2} - \omega S^{\text{in}}_{\text{ch}} Y > M_2(D) - \omega\varphi_0(D).$$

The first (resp. second) condition holds in the region located at the right (resp. left) of the curve Γ_6 (resp. Γ_7). Then, SS5 exists in the region located between the two curves Γ_6 and Γ_7, see Fig. 15. The stability condition of SS5 becomes

$$S^{\text{in}}_{\text{ch}} Y < \varphi_0(D) + \varphi_1(D).$$

Thus, SS5 is stable in the region located at the left of the curve Γ_{10} (see Fig. 15). For SS6, the existence conditions become

$$(1-\omega) S^{\text{in}}_{\text{ch}} Y + S^{\text{in}}_{\text{H}_2} > \phi_2(D), \quad S^{\text{in}}_{\text{ch}} Y > \varphi_0(D) + \varphi_1(D).$$

They hold in the region located at the right of the curves Γ_2 and Γ_{10}, see Fig. 15. Similarly to the section B.2, we have SS6 is stable for all $D \geq \overline{D}$ where $\phi_3(D) \geq 0$. Inversely, when $D < \overline{D}$, Fig. 16(b) shows that $\phi_4(D, S^{\text{in}}_{\text{ch}}) > 0$ for all $S^{\text{in}}_{\text{ch}}$ greater than the abscissa of the green point. Hence, SS6 is stable in the region located at the right of the curve Γ_3, see Fig. 15.

Appendix D. **Table.** In Table 9, we summarize the definitions of surfaces which are the boundaries of different regions of the operating diagrams.

TABLE 9. Definitions of the surfaces Γ_i, $i = 1, \ldots, 18$ where s_0 is the solution of $\psi_0(s_0) = D + a_0$ and s_2^{*i}, $i = 1, 2$ are the solutions of $\Psi(s_2, D) = (1-\omega) Y S^{\text{in}}_{\text{ch}} + Y_4 S^{\text{in}}_{\text{ph}} + S^{\text{in}}_{\text{H}_2}$.

$\Gamma_1 =$	$\left\{ \left(S^{\text{in}}_{\text{ch}}, S^{\text{in}}_{\text{ph}}, S^{\text{in}}_{\text{H}_2}, D \right),\ S^{\text{in}}_{\text{ch}} Y (1-\omega) = \phi_1(D) - S^{\text{in}}_{\text{ph}} Y_4 - S^{\text{in}}_{\text{H}_2} \right\}$
$\Gamma_2 =$	$\left\{ \left(S^{\text{in}}_{\text{ch}}, S^{\text{in}}_{\text{ph}}, S^{\text{in}}_{\text{H}_2}, D \right),\ S^{\text{in}}_{\text{ch}} Y (1-\omega) = \phi_2(D) - S^{\text{in}}_{\text{ph}} Y_4 - S^{\text{in}}_{\text{H}_2} \right\}$
$\Gamma_3 =$	$\left\{ \left(S^{\text{in}}_{\text{ch}}, S^{\text{in}}_{\text{ph}}, S^{\text{in}}_{\text{H}_2}, D \right),\ \phi_4 \left(D, S^{\text{in}}_{\text{ch}}, S^{\text{in}}_{\text{ph}}, S^{\text{in}}_{\text{H}_2} \right) = 0 \right\}$
$\Gamma_4 =$	$\left\{ \left(S^{\text{in}}_{\text{ch}}, S^{\text{in}}_{\text{ph}}, S^{\text{in}}_{\text{H}_2}, D \right),\ r_5 \left(D, S^{\text{in}}_{\text{ch}}, S^{\text{in}}_{\text{ph}}, S^{\text{in}}_{\text{H}_2} \right) = 0 \right\}$
$\Gamma_5 =$	$\left\{ \left(S^{\text{in}}_{\text{ch}}, S^{\text{in}}_{\text{ph}}, S^{\text{in}}_{\text{H}_2}, D \right),\ S^{\text{in}}_{\text{ch}} Y = M_0 \left(D + a_0, S^{\text{in}}_{\text{H}_2} \right) \right\}$
$\Gamma_6 =$	$\left\{ \left(S^{\text{in}}_{\text{ch}}, S^{\text{in}}_{\text{ph}}, S^{\text{in}}_{\text{H}_2}, D \right),\ S^{\text{in}}_{\text{ch}} Y = \varphi_0(D) \right\}$
$\Gamma_7 =$	$\left\{ \left(S^{\text{in}}_{\text{ch}}, S^{\text{in}}_{\text{ph}}, S^{\text{in}}_{\text{H}_2}, D \right),\ S^{\text{in}}_{\text{ch}} Y \omega = \text{S}^{\text{in}}_{\text{H}_2} + \omega\varphi_0(\text{D}) - \text{M}_2(\text{D} + \text{a}_2) \right\}$
$\Gamma_8 =$	$\left\{ \left(S^{\text{in}}_{\text{ch}}, S^{\text{in}}_{\text{ph}}, S^{\text{in}}_{\text{H}_2}, D \right),\ S^{\text{in}}_{\text{ch}} Y = M_0 \left(D + a_0, s_2^{*1} \right) \right\}$
$\Gamma_9 =$	$\left\{ \left(S^{\text{in}}_{\text{ch}}, S^{\text{in}}_{\text{ph}}, S^{\text{in}}_{\text{H}_2}, D \right),\ S^{\text{in}}_{\text{ch}} Y = M_0 \left(D + a_0, s_2^{*2} \right) \right\}$
$\Gamma_{10} =$	$\left\{ \left(S^{\text{in}}_{\text{ch}}, S^{\text{in}}_{\text{ph}}, S^{\text{in}}_{\text{H}_2}, D \right),\ S^{\text{in}}_{\text{ch}} Y = \varphi_0(D) + \varphi_1(D) - S^{\text{in}}_{\text{ph}} Y_4 \right\}$
$\Gamma_{11} =$	$\left\{ \left(S^{\text{in}}_{\text{ch}}, S^{\text{in}}_{\text{ph}}, S^{\text{in}}_{\text{H}_2}, D \right),\ \mu_1 \left(S^{\text{in}}_{\text{ph}} Y_4 + S^{\text{in}}_{\text{ch}} Y - s_0, S^{\text{in}}_{\text{H}_2} - \omega \left(S^{\text{in}}_{\text{ch}} Y - s_0 \right) \right) = D + a_1 \right\}$
$\Gamma_{12} =$	$\left\{ \left(S^{\text{in}}_{\text{ch}}, S^{\text{in}}_{\text{ph}}, S^{\text{in}}_{\text{H}_2}, D \right),\ S^{\text{in}}_{\text{ch}} Y = M_0 \left(D + a_0, s_2^{*1} \right) + M_1 \left(D + a_1, s_2^{*1} \right) - S^{\text{in}}_{\text{ph}} Y_4 \right\}$
$\Gamma_{13} =$	$\left\{ \left(S^{\text{in}}_{\text{ch}}, S^{\text{in}}_{\text{ph}}, S^{\text{in}}_{\text{H}_2}, D \right),\ S^{\text{in}}_{\text{ch}} Y = M_0 \left(D + a_0, s_2^{*2} \right) + M_1 \left(D + a_1, s_2^{*2} \right) - S^{\text{in}}_{\text{ph}} Y_4 \right\}$
$\Gamma_{14} =$	$\left\{ \left(S^{\text{in}}_{\text{ch}}, S^{\text{in}}_{\text{ph}}, S^{\text{in}}_{\text{H}_2}, D \right),\ M_1 \left(D + a_1, M_3 \left(S^{\text{in}}_{\text{ch}} Y, D + a_0 \right) \right) + M_3 \left(S^{\text{in}}_{\text{ch}} Y, D + a_0 \right) = S^{\text{in}}_{\text{ph}} Y_4 + S^{\text{in}}_{\text{H}_2} \right\}$
$\Gamma_{15} =$	$\left\{ \left(S^{\text{in}}_{\text{ch}}, S^{\text{in}}_{\text{ph}}, S^{\text{in}}_{\text{H}_2}, D \right),\ D + a_1 = \mu_1 \left(S^{\text{in}}_{\text{ph}} Y_4, S^{\text{in}}_{\text{H}_2} \right) \right\}$
$\Gamma_{16} =$	$\left\{ \left(S^{\text{in}}_{\text{ch}}, S^{\text{in}}_{\text{ph}}, S^{\text{in}}_{\text{H}_2}, D \right),\ S^{\text{in}}_{\text{ph}} Y_4 + S^{\text{in}}_{\text{H}_2} = M_2(D + a_2) + \varphi_1(D) \right\}$
$\Gamma_{17} =$	$\left\{ \left(S^{\text{in}}_{\text{ch}}, S^{\text{in}}_{\text{ph}}, S^{\text{in}}_{\text{H}_2}, D \right),\ S^{\text{in}}_{\text{ph}} Y_4 = \varphi_1(D) \right\}$
$\Gamma_{18} =$	$\left\{ \left(S^{\text{in}}_{\text{ch}}, S^{\text{in}}_{\text{ph}}, S^{\text{in}}_{\text{H}_2}, D \right),\ D + a_2 = \mu_2 \left(S^{\text{in}}_{\text{H}_2} \right) \right\}$

REFERENCES

[1] N. Abdellatif, R. Fekih-Salem and T. Sari, Competition for a single resource and coexistence of several species in the chemostat, *Math. Biosci. Eng.*, **13** (2016), 631–652.

[2] B. Bar and T. Sari, The operating diagram for a model of competition in a chemostat with an external lethal inhibitor, *Discrete & Contin. Dyn. Syst. Ser. B*, **25** (2020), 2093–2120.

[3] D.J. Batstone, J. Keller, I. Angelidaki, S.V. Kalyhuzhnyi, S.G. Pavlosthathis, A. Rozzi, W.T.M Sanders, H. Siegrist and V.A. Vavilin, The IWA Anaerobic Digestion Model No 1 (ADM1), *Water Sci Technol.*, **45** (2002), 66–73.

[4] T. Bayen and, P. Gajardo, On the steady state optimization of the biogas production in a two-stage anaerobic digestion model, *J. Math. Biol.*, **78** (2019), 1067–1087.

[5] B. Benyahia, T. Sari, B. Cherki and J. Harmand, Bifurcation and stability analysis of a two step model for monitoring anaerobic digestion processes, *J. Proc. Control*, **22** (2012), 1008–1019.

[6] O. Bernard, Z. Hadj-Sadok, D. Dochain, A. Genovesi and J-P. Steyer, Dynamical model development and parameter identification for an anaerobic wastewater treatment process, *Biotechnol. Bioeng.*, **75** (2001), 424–438.

[7] Y. Daoud, N. Abdellatif, T. Sari and J. Harmand, Steady state analysis of a syntrophic model: The effect of a new input substrate concentration, *Math. Model. Nat. Phenom.*, **13** (2018), 1–22.

[8] M. Dellal and B. Bar, Global analysis of a model of competition in the chemostat with internal inhibitor, *Discrete & Contin. Dyn. Syst. Ser. B*, **26** (2021), 1129–1148.

[9] M. Dellal, B. Bar and M. Lakrib, A competition model in the chemostat with allelopathy and substrate inhibition, *Discrete & Contin. Dyn. Syst. Ser. B*, (2021).

[10] M. Dellal, M. Lakrib and T. Sari, The operating diagram of a model of two competitors in a chemostat with an external inhibitor, *Math. Biosci.*, **302** (2018), 27–45.

[11] M. El-Hajji, F. Mazenc and J. Harmand, A mathematical study of a syntrophic relationship of a model of anaerobic digestion process, *Math. Biosci. Eng.*, **7** (2010), 641–656.

[12] M. El-Hajji, N. Chorfi and M. Jleli, Mathematical modelling and analysis for a three-tiered microbial food web in a chemostat, *Electron. J. Differential Equations*, **255** (2017), 255.

[13] R. Fekih-Salem, C. Lobry and T. Sari, A density-dependent model of competition for one resource in the chemostat, *Math. Biosci.*, **286** (2017), 104–122.

[14] R. Fekih-Salem, Y. Daoud, N. Abdellatif and T. Sari, A mathematical model of anaerobic digestion with syntrophic relationship, substrate inhibition and distinct removal rates, *To appear in SIAM J. Appl. Dyn. Syst. SIADS*, (2021) *hal-02085693*.

[15] J. Harmand, C. Lobry, A. Rapaport and T. Sari, The Chemostat: Mathematical Theory of Microorganism Cultures, vol. 1, *Chemical Eng. Ser., Chemostat Bioprocesses Set, Wiley, New York.*, (2017).

[16] S-B. Hsu and Y-T. Yang, Theory of a microfluidic serial dilution bioreactor for growth of planktonic and biofilm populations, *J. Math. Biol.*, **72** (2016), 1401–27.

[17] Z. Khedim, B. Benyahia, B. Cherki, T. Sari and J. Harmand, Effect of control parameters on biogas production during the anaerobic digestion of protein-rich substrates, *Appl. Math. Model.*, **61** (2018), 351–376.

[18] MAPLE, version 17.0.0.0, *Waterloo Maple Inc.*, Waterloo, Ontario (2018).

[19] T. Mtar, R. Fekih-Salem and T. Sari, Interspecific density-dependent model of predator-prey relationship in the chemostat, *Int. J. Biomath.*, **14** (2021), 2050086, 22 pp.

[20] S. Nouaoura, N. Abdellatif, R. Fekih-Salem and T. Sari, Mathematical analysis of a three-tiered model of anaerobic digestion, *SIAM - Journal on Applied Mathematics (SIAP)*, (2021), hal-02540350.

[21] S. Nouaoura, R. Fekih-Salem, N. Abdellatif and T. Sari, Mathematical analysis of a three-tiered food-web in the chemostat, *Discrete & Contin. Dyn. Syst. Ser. B*, (2020).

[22] S. Pavlou, Computing operating diagrams of bioreactors, *J. Biotechnol.*, **71** (1999), 7–16.

[23] T. Sari and B. Benyahia, The operating diagram for a two-step anaerobic digestion model, to appear in Nonlinear Dynamics (2020), hal-02557464.

[24] T. Sari, M. El-Hajji and J. Harmand, The mathematical analysis of a syntrophic relationship between two microbial species in a chemostat, *Math. Biosci. Eng.*, **9** (2012), 627–645.

[25] T. Sari and J. Harmand, A model of a syntrophic relationship between two microbial species in a chemostat including maintenance, *Math. Biosci.*, **275** (2016), 1–9.

[26] T. Sari and M.J. Wade, Generalised approach to modelling a three-tiered microbial food-web, *Math. Biosci.*, **291** (2017), 21–37.
[27] M. Sbarciog, M. Loccufier and E. Noldus, Determination of appropriate operating strategies for anaerobic digestion systems, *Biochem. Eng. J.*, **51** (2010), 180–188.
[28] H.L. Smith and P. Waltman, The Theory of the Chemostat: Dynamics of Microbial Competition, *Cambridge University Press, Cambridge, UK*, (1995).
[29] S. Sobieszek, M.J. Wade and G.S.K. Wolkowicz, Rich dynamics of a three-tiered anaerobic food-web in a chemostat with multiple substrate inflow, *Math. Biosci. Eng.*, **17** (2020), 7045–7073.
[30] M.J. Wade, R.W. Pattinson, N.G. Parker and J. Dolfing, Emergent behaviour in a chlorophenol-mineralising three-tiered microbial "food web", *J. Theor. Biol.*, **389** (2016), 171–186.
[31] M. Weedermann, Analysis of a model for the effects of an external toxin on anaerobic digestion, *Math. Biosci. Eng.*, **9** (2012), 445–459.
[32] M. Weedermann, G.S.K. Wolkowicz and J. Sasara, Optimal biogas production in a model for anaerobic digestion, *Nonlinear Dyn.*, **81** (2015), 1097–1112.
[33] A. Xu, J. Dolfing, T.P. Curtis, G. Montague and E. Martin, Maintenance affects the stability of a two-tiered microbial "food chain"?, *J. Theor. Biol.*, **276** (2011), 35–41.

E-mail address: sarra.nouaoura@enit.utm.tn
E-mail address: radhouene.fekihsalem@isima.rnu.tn
E-mail address: nahla.abdellatif@ensi-uma.tn
E-mail address: tewfik.sari@inrae.fr